IEEE Access
Multidisciplinary | Rapid Review | Open Access Journal

Received May 21, 2019, accepted May 29, 2019, date of publication June 3, 2019, date of current version June 18, 2019.

Digital Object Identifier 10.1109/ACCESS.2019.2920415

Disturbance-Estimation Based Adaptive Backstepping Fault-Tolerant Synchronization Control for a Dual Redundant Hydraulic Actuation System With Internal Leakage Faults

TING LI[1,2], TING YANG[1,2], YUYAN CAO[1], RONG XIE[1], AND XINMIN WANG[1]
[1]School of Automation, Northwestern Polytechnical University, Xi'an 710129, China
[2]State Key Laboratory of Robotics and System, Harbin Institute of Technology, Harbin 150001, China

Corresponding author: Ting Li (liting513@mail.nwpu.edu.cn)

This work was supported in part by the National Natural Science Foundation under Grant 61703341, in part by the China Postdoctoral Science Foundation under Grant 2018M633576, in part by the Natural Science Basic Research Plan in Shaanxi Province of China under Grant 2018JQ6008, in part by the State Key Laboratory of Robotics and System (HIT) under Grant SKLRS-2018-KF-13, and in part by the Shaanxi Postdoctoral Science Foundation under Grant 2018BSHYDZZ65.

ABSTRACT In this paper, a fault-tolerant synchronization control (FTSC) algorithm is proposed to deal with the position tracking control problem for a dual redundant hydraulic actuation system (DRHAS) working on active/active (A/A) mode and suffering from internal leakage faults, large disturbances, and force fighting between actuators. Specifically, two reference trajectories are introduced and a novel nonlinear model for the DRHAS is developed to facilitate the synthesis of position tracking control and force synchronization control. Then, a nonlinear FTSC algorithm is proposed by incorporating adaptive control and disturbance rejection control into the backstepping design. In which, a simple reconfiguration mechanism based on faulty parameters online adaptation is adopted to accommodate the faults. The matched and unmatched disturbances in both actuators are estimated by constructing four extended state observers (ESOs) and are compensated in a feedforward way. The stability analysis indicates that the proposed control algorithm can ensure prescribed tracking performance for the system under internal leakage faults and time-varying disturbances, and can make the tracking error of the faulty system converge to zero asymptotically under constant disturbances. Finally, the effectiveness of the proposed control algorithm is verified through comparative simulations.

INDEX TERMS Dual redundant hydraulic actuation system, fault-tolerant control, disturbance rejection control, synchronization control, adaptive backstepping.

I. INTRODUCTION

The redundant hydraulic actuation systems (RHAS) have been universally adopted to drive the primary control surfaces of the modern airplanes. For example, both ailerons of the Airbus A320 are driven by a dual redundant hydraulic actuation system (DRHAS), and the rudder of the plane is driven by a triply redundant hydraulic actuation system (TRHAS) [1].

The associate editor coordinating the review of this manuscript and approving it for publication was Jianyong Yao.

In a typical RHAS configuration, several parallelly connected hydraulic actuators (HA) operate on A/A mode to deflect the control surface, and their outputs are summed by force [2]. A major issue that affects the position tracking accuracy of such system is the force fighting between HA channels, namely the HAs output non-synchronous forces due to reasons such as manufacturing tolerances and individual nonlinear property, and then they fight against each other to find an equilibrium point to drive the common control surface [3]. To reduce force fighting and realize high-accuracy positon tracking control for RHAS, some force

equalization control methods such as pressure differential equalization control [4], decoupling control [5], and motion state synchronization control [6], [7] have been proposed in recent years.

By employing the control strategies mentioned above, the force fighting problem was proved to be reduced effectively. However, most of the existing results have neglected the impact of faults on the performance of the RHAS. A fault with greatest concerns is the internal leakage in hydraulic cylinder, which can impair the system performance or even make the system unstable if they are not compensated properly [8]. On the other hand, the internal leakage faults occurring in one or more HA channels can cause changes on dynamic response of actuators and aggravate the non-synchronous force outputs, which eventually results in more serious force fighting problem. Since internal leakage faults are inevitable, it is very meaningful to develop a control scheme that takes into account both control problems, i.e., the force equalization control and the fault-tolerant control (FTC).

Many schemes such as Kalman filter-based schemes [9], [10], wavelet-based schemes [11], neural network(NN)-based schemes [12] and observer-based schemes [13] have been studied extensively to handle the internal leakage fault detection problem in HAs. However, to the best of the authors' knowledge, research on FTC problem for HAs especially for RHAS subject to internal leakage faults is still very limited. In [14], an FTC algorithm based on stochastic parameter estimation was presented for an HA with internal leakage fault. In [15], an adaptive robust FTC scheme based on faulty parameter adaption was proposed for a single-rod HA. In [16], a set of local controllers were designed to compensate for different levels of leakage in HA cylinder by employing quantitative feedback theory. In [17], a set of local fuzzy PI controllers with respect to different RHAS operating conditions were constructed and a strategy for synthesizing the available controllers was developed based on the fault information obtained from a novel disturbance-decoupled observer. In [18], several performance degradation reference models corresponding to different fault levels were constructed for a dissimilar redundant actuation system in active/standby mode and a series of adaptive fuzzy controllers were designed accordingly to limit the system performance degradation. Among these methods, the schemes [16]–[18] are linear control strategies without consideration of disturbances and it should be noted that a high position tracking accuracy cannot be achieved with a linear controller due to the high nonlinearity of the HA [19]. Furthermore, the nonlinear controllers in [14], [15] have neglected the matched disturbances in actuators.

In practice, the positon tracking accuracy of the RHAS is affected not only by faults or force fighting between HA channels but also by matched and unmatched disturbances, such as the modeling error of the pressure dynamics and the unmolded load force of the cylinder dynamics. However, to the best of the authors' knowledge, few control schemes for the RHAS have considered the matched and unmatched disturbances simultaneously. Recently, to achieve high-accuracy position tracking performance, active disturbance rejection control (ADRC) has been extensively studied to cope with large disturbances in the HA. The main idea of the ADRC is to estimate the disturbances from measurable states and take a control action to compensate the effects of the disturbances in a feedforward way. In [20], a nonlinear disturbance observer was designed to estimate the matched disturbance by assuming the derivative of the disturbance was zero. In [21], the periodic-like disturbances were approximated by applying Fourier series expansion and an adaptive repetitive controller was constructed to learn and compensate the disturbances. In [22], an adaptive extended state observer driven by the velocity signal was constructed to estimate the unmatched disturbance and therefore the estimation result is easily polluted by severe measurement noise existed in the velocity signal. In [23], a disturbance observer in the form of a second-order high-pass filter was constructed, but the upper bound of the estimation error was required to be known to design the compensation control strategy. In [24], the matched and unmatched disturbances were estimated by high-gain observers, and two auxiliary states instead of the derivate of the measured signal were used to avoid the amplification of the measurement noise. In [25], two multilayer NNs estimators were designed to deal with the matched and unmatched disturbances and an asymptotic tracking performance can be achieved by integrating with the adaptive robust integral of the sign of the error (RISE) feedback control approach.

Motivated by the above discussions, a disturbance-estimation based adaptive backstepping fault-tolerant synchronization control (DAFTSC) algorithm is proposed for a DRHAS operating on A/A mode. Firstly, inspired by [5], two reference trajectories are employed and a novel nonlinear model is developed to facilitate the controller design for integrating two control objectives, i.e., the positon tracking and the force synchronization. Then, a DAFTSC controller is developed by incorporating adaptive control and ESO-based ADRC into backstepping design. In which, the internal leakage faults in both HA channels are treated as faulty parameters variation and are effectively accommodated by a simple reconfiguration design based on faulty parameters online adaptation. Moreover, to reduce the effects of large disturbances on control performance, the matched and unmatched disturbances in both HA channels are estimated by four linear ESOs and are compensated in a feedforward way. By employing Lyapunov stability theory, it shows that the proposed control algorithm can ensure the closed-loop system to achieve a prescribed tracking performance under internal leakage faults and time-varying disturbances, and can make the final system tracking error converge to zero asymptotically under faults and constant disturbances. The contributions of the paper are listed below:

1) A novel nonlinear model of a DRHAS is proposed to facilitate the synthesis of two control objectives, namely the position tracking and the force synchronization.

2) A simple reconfiguration mechanism based on faulty parameters online adaptation is designed to accommodate the faults as soon as possible.

3) The matched and unmatched disturbances in both HA channels are estimated by constructing four linear ESOs, and the effects of the disturbances on position tracking performance of the system are greatly attenuated by employing a feedforward compensation strategy.

4) A DAFTSC controller which incorporates adaptive control and ESO-based ADRC into backstepping design is proposed to deal with the control problem of the DRHAS in the present of internal leakage faults, force fighting and large disturbances.

The remaining of the paper is organized as follows: A nonlinear model for the DRHAS and a formulation of the control problem are given in Section II. The internal leakage faults estimation, the ESO-based disturbances estimation, the controller design and the stability analysis for the closed-loop control system are presented in Section III. Comparative simulation studies are shown in Section IV. Finally, a conclusion is given in Section V.

Notations: $diag(\cdot)$ represents a diagonal matrix. $\boldsymbol{I}_n$ and $\boldsymbol{O}_n$ denote the $n \times n$ identity matrix and $n \times n$ zero matrix, respectively. $\boldsymbol{M}^T$ and $\boldsymbol{M}^{-1}$ denote the transpose and the inverse of the matrix $\boldsymbol{M}$, respectively. $\lambda_{\max}(\cdot)$ and $\lambda_{\min}(\cdot)$ stand for the maximal and minimal eigenvalues of a matrix, respectively. $\|\cdot\|$ represents the Euclidean norm of a vector or the spectral norm of a matrix, and $\|\cdot\|_{\max}$ stands for their maximum values accordingly.

II. NONLINEAR MODEL AND PROBLEM STATEMENT

The structure of a DRHAS operating on A/A mode is shown in Figure 1. Two HAs powered by different hydraulic power sources (marked in blue and green, respectively) are connected to a common control surface, and each HA mainly consists of an electro-hydraulic servovalve and a single-rod hydraulic cylinder.

A. NONLINEAR MODEL OF THE SINGLE-CHANNEL HA

The force balance equation of a hydraulic cylinder is shown as follows:

$$\ddot{x}_{hi} = \frac{1}{m_{hi}}[A_1 P_{hi1} - A_2 P_{hi2} - B_{hi}\dot{x}_{hi} - F_{hi} - d_i] \quad (1)$$

where x_{hi} and m_{hi} are piston rod displacement and piston mass. Throughout this paper the subscript i $(i = 1, 2)$ in italic type denotes the two HAs in the DRHAS. A_1 is the piston area of the active chamber and A_2 is the piston area of the passive chamber. P_{hi1} and P_{hi2} are the pressures of the two chambers. B_{hi} is the damping coefficient, F_{hi} is the external load of the cylinder, and d_i is the unmatched disturbance that includes unmodeled load force and external disturbances.

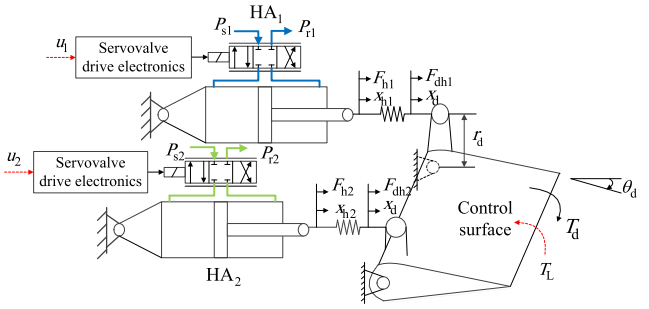

FIGURE 1. Structure diagram of a DRHAS operating on A/A mode.

Suppose both HAs in the DRHAS are connected rigidly to the control surface and F_{hi} can be described as

$$F_{hi} = K_{hi}(x_{hi} - x_d) \quad (2)$$

where K_{hi} is the connect stiffness, x_d is the linear displacement of the control surface which can be approximately represented as $x_d = r_d\theta_d$ when the control surface angle θ_d varies within a small range, and r_d is the radial distance of the control surface.

The pressure dynamics of the two chambers are represented by [26]

$$\dot{P}_{hi1} = \frac{\beta_e}{V_{hi1}}(-A_1\dot{x}_{hi} - q_{hi} + Q_{hi1} + q_{ui1}), \quad (3)$$

$$\dot{P}_{hi2} = \frac{\beta_e}{V_{hi2}}(A_2\dot{x}_{hi} + q_{hi} - Q_{hi2} - q_{ui2}) \quad (4)$$

where β_e is the effective oil bulk modulus, $V_{hi1} = V_{10} + A_1 x_{hi}$ and $V_{hi2} = V_{20} - A_2 x_{hi}$ are the volumes of the chambers, and V_{10} and V_{20} are their initial volumes. q_{hi} is the internal leakage of the actuator. Q_{hi1} is the supply flow rate of the active chamber, and Q_{hi2} is the return flow rate of the passive chamber. q_{ui1} and q_{ui2} are the matched disturbances caused by unmodeled pressure dynamics and parameter deviations, which can significantly affect the dynamics of the HA [26].

Since the dynamics of the valve is much faster than the other parts of the system, its dynamics is neglected without significantly affecting the control performance [27]. Therefore, we assume that the servovalve displacement x_{vi} is proportional to the control input u_i, i.e., $x_{vi} = k_{ui}u_i$, and the flow rates Q_{hi1} and Q_{hi2} can be calculated by

$$Q_{hi1} = k_q k_{ui} R_{hi1} u_i, \quad (5)$$

$$Q_{hi2} = k_q k_{ui} R_{hi2} u_i \quad (6)$$

where k_q is the flow rate gain, k_{ui} is the servovalve gain, and R_{hi1}, R_{hi2} are defined as [28]

$$R_{hi1} = s(u_i)\sqrt{P_{si} - P_{hi1}} + s(-u_i)\sqrt{P_{hi1} - P_{ri}}, \quad (7)$$

$$R_{hi2} = s(u_i)\sqrt{P_{hi2} - P_{ri}} + s(-u_i)\sqrt{P_{si} - P_{hi2}} \quad (8)$$

and the function $s(x)$ is defined as

$$s(x) \triangleq \begin{cases} 1 & x \geq 0 \\ 0 & x < 0 \end{cases}. \quad (9)$$

The internal leakage in the cylinder can be modeled by

$$q_{hi} = C_{ii}(P_{hi1} - P_{hi2}) + C_{ti}\sqrt{|P_{hi1} - P_{hi2}|}\,\mathrm{sgn}(P_{hi1} - P_{hi2}) \tag{10}$$

where C_{ii} is the normal internal leakage coefficient, and C_{ti} is the unknown fault internal leakage coefficient need to be estimated.

According to (1)–(10), define the state variables as $\boldsymbol{x}_i = [x_{i1}, x_{i2}, x_{i3}]^T = [x_{hi}, \dot{x}_{hi}, A_1P_{hi1} - A_2P_{hi2}]^T$, then the state space model of an HA can be written as

$$\begin{cases} \dot{x}_{i1} = x_{i2} \\ \dot{x}_{i2} = -\dfrac{K_{hi}}{m_{hi}}x_{i1} - \dfrac{B_{hi}}{m_{hi}}x_{i2} + \dfrac{1}{m_{hi}}x_{i3} + \dfrac{K_{hi}r_d}{m_{hi}}\theta_d - \dfrac{1}{m_{hi}}d_i \\ \dot{x}_{i3} = f_{hi1}u_i - f_{hi2} - C_{ti}f_{hi3} + q_i \end{cases} \tag{11}$$

where

$$\begin{aligned} f_{hi1} &= \frac{A_1\beta_e}{V_{hi1}}k_q k_{ui}R_{hi1} + \frac{A_2\beta_e}{V_{hi2}}k_q k_{ui}R_{hi2}, \\ f_{hi2} &= \frac{A_1\beta_e}{V_{hi1}}[A_1\dot{x}_{hi} + C_{ii}(P_{hi1} - P_{hi2})] \\ &\quad + \frac{A_2\beta_e}{V_{hi2}}[A_2\dot{x}_{hi} + C_{ii}(P_{hi1} - P_{hi2})], \\ f_{hi3} &= C_{ti}\left(\frac{A_1\beta_e}{V_{hi1}} + \frac{A_2\beta_e}{V_{hi2}}\right)\sqrt{|P_{hi1} - P_{hi2}|}\,\mathrm{sgn}(P_{hi1} - P_{hi2}), \end{aligned}$$

and

$$q_i = \frac{A_1\beta_e}{V_{hi1}}q_{ui1} + \frac{A_2\beta_e}{V_{hi2}}q_{ui2}.$$

Assumption 1: The disturbances d_i, q_i and their time derivatives are bounded; The chamber pressures of the cylinder P_{hi1}, P_{hi2} are bounded and satisfy $P_{ri} < P_{hi1} < P_{si}$ and $P_{ri} < P_{hi2} < P_{si}$, respectively.

B. NONLINEAR MODEL OF THE DRHAS

Based on the model of the single-channel HA, the model of the DRHAS can be easily derived. Define the state variables as

$$\begin{aligned} \boldsymbol{x} &= \begin{bmatrix} x_{11}, x_{12}, x_{13} \\ x_{21}, x_{22}, x_{23} \end{bmatrix}^T \\ &\triangleq \begin{bmatrix} x_{h1}, \dot{x}_{h1}, A_1P_{h11} - A_2P_{h12} \\ x_{h2}, \dot{x}_{h2}, A_1P_{h21} - A_2P_{h22} \end{bmatrix}^T, \end{aligned} \tag{12}$$

then the state space of the DRHAS can be written as

$$\begin{cases} \begin{bmatrix} \dot{x}_{11} \\ \dot{x}_{21} \end{bmatrix} = \begin{bmatrix} x_{12} \\ x_{22} \end{bmatrix} \\ \begin{bmatrix} \dot{x}_{12} \\ \dot{x}_{22} \end{bmatrix} = -\boldsymbol{H}_1\begin{bmatrix} x_{11} \\ x_{21} \end{bmatrix} - \boldsymbol{H}_2\begin{bmatrix} x_{12} \\ x_{22} \end{bmatrix} + \boldsymbol{H}_3\begin{bmatrix} x_{13} \\ x_{23} \end{bmatrix} \\ \qquad + \boldsymbol{H}_4\boldsymbol{x}_c - \boldsymbol{H}_3\boldsymbol{d} \\ \begin{bmatrix} \dot{x}_{13} \\ \dot{x}_{23} \end{bmatrix} = \boldsymbol{F}_1\boldsymbol{u} - \boldsymbol{F}_2 - \boldsymbol{F}_3\theta + \boldsymbol{H}_q \end{cases} \tag{13}$$

where

$$\begin{aligned} \boldsymbol{H}_1 &= diag(K_{h1}/m_{h1}, K_{h2}/m_{h2}), \\ \boldsymbol{H}_2 &= diag(B_{h1}/m_{h1}, B_{h2}/m_{h2}), \\ \boldsymbol{H}_3 &= diag(1/m_{h1}, 1/m_{h2}), \\ \boldsymbol{H}_4 &= diag(K_{h1}r_d/m_{h1}, K_{h2}r_d/m_{h2}), \quad \boldsymbol{d} = [d_1, d_2]^T, \\ \boldsymbol{F}_1 &= diag(f_{h11}, f_{h21}), \quad \boldsymbol{F}_2 = [f_{h12}, f_{h22}]^T, \\ \boldsymbol{F}_3 &= diag(f_{h13}, f_{h23}), \\ \boldsymbol{H}_q &= [q_1, q_2]^T, \quad \boldsymbol{\theta} = [C_{t1}, C_{t2}]^T \end{aligned}$$

is a vector of unknown internal leakage fault parameters, $\boldsymbol{u} = [u_1, u_2]^T$ is a vector of system inputs, and $\boldsymbol{x}_c = [\theta_d, \theta_d]^T$ is the coupling term between two HAs.

Assumption 2: The fault parameter vector $\boldsymbol{\theta}$ satisfy

$$\boldsymbol{\theta}_{\min} \le \boldsymbol{\theta} \le \boldsymbol{\theta}_{\max} \tag{14}$$

where $\boldsymbol{\theta}_{\min}$ and $\boldsymbol{\theta}_{\max}$ are known constant vectors, $\boldsymbol{\theta}_{\min} = [\theta_{1\min}, \theta_{2\min}]^T$, and $\boldsymbol{\theta}_{\max} = [\theta_{1\max}, \theta_{2\max}]^T$.

Remark 1: Noting Assumption 1, equations (7) and (8), we have $R_{hi1} > 0, R_{hi2} > 0$. Thus, the inequality $f_{hi1} > 0$ holds and the matrix $\boldsymbol{F}_1$ is reversible.

Suppose the DRHAS is working on A/A mode and the outputs of the two HAs are summed by force. Then the dynamics of the control surface can be represented as

$$(F_{dh1} + F_{dh2})r_d = J_d\ddot{\theta}_d + \beta_d\dot{\theta}_d + T_L \tag{15}$$

where the driving forces $F_{dh1} = F_{h1}$, $F_{dh2} = F_{h2}$, J_d is the moment of inertia, β_d is the damping coefficient, and T_L is the load torque.

Define the system outputs as $y_1 = \theta_d, y_2 = \dot{\theta}_d$, and then according to (2) and (15), the output equation of the DRHAS can be written as

$$\begin{cases} \dot{y}_1 = y_2 \\ \dot{y}_2 = \dfrac{r_d}{J_d}(K_{h1}x_{11} + K_{h2}x_{12}) - \dfrac{r_d^2}{J_d}(K_{h1} + K_{h2})y_1 \\ \qquad -\dfrac{\beta_d}{J_d}y_2 - \dfrac{1}{J_d}T_L. \end{cases} \tag{16}$$

C. MODEL TRANSFORMATION AND PROBLEM STATEMENT

For the DRHAS (13) and (16), the goal of this paper is to design a fault-tolerant synchronization control scheme to ensure that

1) The output control surface deflection angle θ_d can track the reference trajectory θ_r accurately, especially in the present of internal leakage faults, matched and unmatched disturbances.

2) Synchronized force outputs for HAs can be maintained to reduce the force fighting effectively no matter in fault-free or faulty cases.

To achieve the above control objectives and simplify the nonlinear controller design, two reference trajectories for the controller are introduced [5].

Firstly, a reference trajectory x_{r1} which is derived from (16) is introduced for positon tracking control.

Assumption 3: The reference trajectory θ_r is C^5 continuous and bounded.

Theorem 1 [29]: For function $f_1(x_{11}, x_{21}) = K_{h1}x_{11} + K_{h2}x_{21}$, the output deflection angle of the control surface θ_d can track the reference trajectory θ_r accurately if the function $f_1(x_{11}, x_{21})$ can track the reference trajectory x_{r1} which satisfies

$$x_{r1} = \frac{J_d}{r_d}[\frac{r_d^2}{J_d}(K_{h1} + K_{h2})y_1 + \frac{\beta_d}{J_d}y_2 + \frac{1}{J_d}T_L + \dot{\alpha}_{r1} - k_2 z_2 - z_1]. \quad (17)$$

where, $\alpha_{r1} = -k_1 z_1 + \dot{\theta}_r$ is a virtue control input, $z_1 = y_1 - \theta_r$ and $z_2 = y_2 - \alpha_{r1}$ are error variables, k_1 and k_2 are positive constants. The proof of the theorem can refer to reference [29].

Then, a reference trajectory x_{r2} is employed for force outputs synchronization control for two HAs.

Define a function as $f_2(x_{11}, x_{21}) = K_{h1}x_{11} - K_{h2}x_{21}$ and a reference trajectory $x_{r2} = (K_{h1} - K_{h2})r_d\theta_d$. Based on (2), the fighting force between two HAs can be represented as

$$\begin{aligned}\Delta F &= F_{h1} - F_{h2} \\ &= (K_{h1}x_{11} - K_{h2}x_{21}) - (K_{h1} - K_{h2})r_d\theta_d \end{aligned} \quad (18)$$

and it can be observed that the fighting force ΔF will approach to zero to achieve force outputs synchronization when the function $f_2(x_{11}, x_{21})$ can track the reference trajectory x_{r2} accurately.

Remark 2: It is easy to deduce that the actual deflection angle θ_d and its time derivative $\dot{\theta}_d$ are bounded, and the reference trajectories x_{r1} and x_{r2} are both C^3 continuous and bounded. Readers can refer to [29] for more detailed information.

Based on the two reference trajectories, a new state vector is defined as follows:

$$\boldsymbol{f}(x_{11}, x_{21}, t) = \begin{bmatrix} f_1(x_{11}, x_{21}) \\ f_2(x_{11}, x_{21}) \end{bmatrix} = \boldsymbol{T}\begin{bmatrix} x_{11} \\ x_{21} \end{bmatrix} \quad (19)$$

where $\boldsymbol{T} = \begin{bmatrix} K_{h1} & K_{h2} \\ K_{h1} & -K_{h2} \end{bmatrix}$ is a linear transformation matrix.

Then, by introducing the linear transformation $\boldsymbol{T}$ for the first two equations of (13), a new state-space model for the DRHAS can be obtained as

$$\begin{cases} \dot{\boldsymbol{f}}(x_{11}, x_{21}, t) = \boldsymbol{f}(x_{12}, x_{22}, t) \\ \dot{\boldsymbol{f}}(x_{12}, x_{22}, t) = -\boldsymbol{M}_1\boldsymbol{f}(x_{11}, x_{21}, t) - \boldsymbol{M}_2\boldsymbol{f}(x_{12}, x_{22}, t) \\ \qquad\qquad +\boldsymbol{M}_3\boldsymbol{x}_3 + \boldsymbol{M}_4\boldsymbol{x}_c + \boldsymbol{T}\boldsymbol{H}_d \\ \dot{\boldsymbol{x}}_3 = \boldsymbol{F}_1\boldsymbol{u} - \boldsymbol{F}_2 - \boldsymbol{F}_3\boldsymbol{\theta} + \boldsymbol{H}_q \end{cases} \quad (20)$$

where $\boldsymbol{M}_1 = \boldsymbol{T}\boldsymbol{H}_1\boldsymbol{T}^{-1}$, $\boldsymbol{M}_2 = \boldsymbol{T}\boldsymbol{H}_2\boldsymbol{T}^{-1}$, $\boldsymbol{M}_3 = \boldsymbol{T}\boldsymbol{H}_3$, $\boldsymbol{M}_4 = \boldsymbol{T}\boldsymbol{H}_4$, $\boldsymbol{H}_d = -\boldsymbol{H}_3\boldsymbol{d}$.

Remark 3: Based on the definitions of $\boldsymbol{T}$, $\boldsymbol{H}_3$ and $\boldsymbol{M}_3$, it can be found that $\boldsymbol{M}_3$ is reversible.

To facilitate the use of backstepping method for controller design, define a new state variable as $\bar{\boldsymbol{x}}_3 = \boldsymbol{M}_3\boldsymbol{x}_3$ and the state-space model (20) can be represented in the following semi-strict-feedback form [30]:

$$\begin{cases} \dot{\boldsymbol{f}}(x_{11}, x_{21}, t) = \boldsymbol{f}(x_{12}, x_{22}, t) \\ \dot{\boldsymbol{f}}(x_{12}, x_{22}, t) = -\boldsymbol{M}_1\boldsymbol{f}(x_{11}, x_{21}, t) - \boldsymbol{M}_2\boldsymbol{f}(x_{12}, x_{22}, t) \\ \qquad\qquad +\bar{\boldsymbol{x}}_3 + \boldsymbol{M}_4\boldsymbol{x}_c + \boldsymbol{T}\boldsymbol{H}_d \\ \dot{\bar{\boldsymbol{x}}}_3 = \boldsymbol{M}_3\boldsymbol{F}_1\boldsymbol{u} - \boldsymbol{M}_3\boldsymbol{F}_2 - \boldsymbol{M}_3\boldsymbol{F}_3\boldsymbol{\theta} + \boldsymbol{M}_3\boldsymbol{H}_q. \end{cases} \quad (21)$$

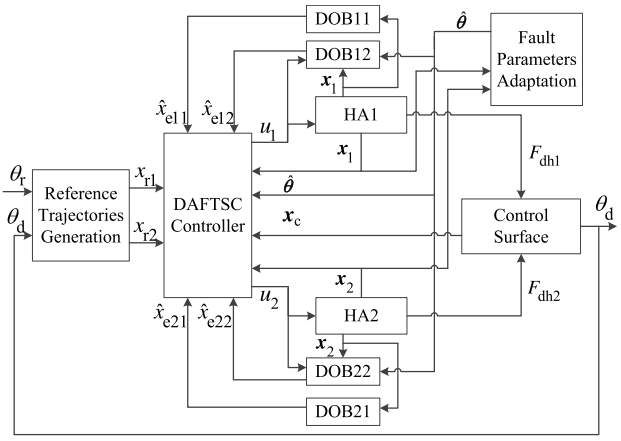

FIGURE 2. Structure diagram of the proposed DAFTSC algorithm.

Therefore, for the DRHAS (21) subject to internal leakage faults $\boldsymbol{\theta}$, matched disturbance $\boldsymbol{H}_q$ and unmatched disturbance $\boldsymbol{H}_d$, the aforementioned control objectives can be transformed into the following new ones:

1) The state variable $f_1(x_{11}, x_{21})$ can track the reference trajectory x_{r1} accurately.

2) The state variable $f_2(x_{11}, x_{21})$ can track the reference trajectory x_{r2} accurately.

III. DAFTSC ALGORITHM

In this section, a DAFTSC algorithm is proposed to fulfill the aforementioned control objectives. The magnitude of the internal leakage fault in each HA channel is obtained by online adaptation, and the matched and unmatched disturbances in the system are estimated by constructing four linear ESOs [26], [31], [32] through full state feedback. A nonlinear controller employing the estimated information is synthesized by backstepping technology. A structure diagram of the proposed algorithm is illustrated in Figure 2.

A. FAULTY PARAMETERS ONLINE ADAPTATION

To estimate the unknown fault parameter vector $\boldsymbol{\theta}$, an online adaptation law is chosen as

$$\dot{\hat{\boldsymbol{\theta}}} = \mathrm{Proj}_{\hat{\boldsymbol{\theta}}}(\boldsymbol{\Gamma}\boldsymbol{\sigma}) \quad (22)$$

where $\boldsymbol{\Gamma} = \mathrm{diag}(\Gamma_1, \Gamma_2)$ is a diagonal positive definite matrix to control the parameter adaptation rates, $\boldsymbol{\sigma}$ is an adaptation function, which will be obtained by synthesizing the Lyapunov stability analysis later, and $\mathrm{Proj}_{\hat{\theta}_i}(\cdot_i)$ is

a discontinuous projection mapping which is defined as [33]:

$$\mathrm{Proj}_{\hat{\theta}_i}(\cdot_i) = \begin{cases} 0 & \text{if } \hat{\theta}_i = \theta_{i\max} \text{ and } \cdot_i > 0 \\ 0 & \text{if } \hat{\theta}_i = \theta_{i\min} \text{ and } \cdot_i < 0 \\ \cdot_i & \text{otherwise} \end{cases}. \quad (23)$$

The projection mapping in (23) can ensure the parameters adaption process has the following properties:

$$\text{P1}.\hat{\boldsymbol{\theta}} \in \Omega_{\hat{\boldsymbol{\theta}}} \triangleq \{\hat{\boldsymbol{\theta}} : \boldsymbol{\theta}_{\min} \le \hat{\boldsymbol{\theta}} \le \boldsymbol{\theta}_{\max}\}, \quad (24)$$

$$\text{P2}.\tilde{\boldsymbol{\theta}}^T[\boldsymbol{\Gamma}^{-1}\mathrm{Proj}_{\hat{\boldsymbol{\theta}}}(\boldsymbol{\Gamma}\boldsymbol{\sigma}) - \boldsymbol{\sigma}] \le 0, \quad \forall\, \boldsymbol{\sigma}. \quad (25)$$

B. EXTENDED-OBSERVER-BASED DISTURBANCE ESTIMATION

Two linear ESOs which are denoted as DOB11 and DOB21 are constructed to estimate the unmatched disturbance in HA1 and HA2 respectively.

Define an extended state vector as $\boldsymbol{x}_{ei1} = [x_{i1}, x_{i2}, x_{ei1}]^T = [x_{hi}, \dot{x}_{hi}, -d_i/m_{hi}]^T$ and let $\dot{x}_{ei1} = h_{ei1}(t)$, here $h_{ei1}(t)$ is an unknown but bounded function which denotes the change rate of the unmatched disturbance. Then, based on the first two equations of (11), an extended state-space equation can be written as follows:

$$\begin{cases} \dot{\boldsymbol{x}}_{ei1} = \boldsymbol{A}_{ei1}\boldsymbol{x}_{ei1} + \boldsymbol{\Phi}_{ei1} + \boldsymbol{H}_{ei1} \\ y_{ei1} = \boldsymbol{C}_{ei1}\boldsymbol{x}_{ei1} \end{cases} \quad (26)$$

where $\boldsymbol{A}_{ei1} = \begin{bmatrix} 0 & 1 & 0 \\ 0 & 0 & 1 \\ 0 & 0 & 0 \end{bmatrix}$, $\boldsymbol{\Phi}_{ei1} = \begin{bmatrix} 0 \\ \phi_{i2} \\ 0 \end{bmatrix}$, $\boldsymbol{H}_{ei1} = \begin{bmatrix} 0 \\ 0 \\ h_{ei1}(t) \end{bmatrix}$, $\phi_{i2} = -\frac{K_{hi}}{m_{hi}}x_{i1} - \frac{B_{hi}}{m_{hi}}x_{i2} + \frac{1}{m_{hi}}x_{i3} + \frac{K_{hi}r_d}{m_{hi}}\theta_d$, and $\boldsymbol{C}_{ei1} = [1, 0, 0]$.

According to (26), the DOB11/DOB21 can be designed as

$$\dot{\hat{\boldsymbol{x}}}_{ei1} = \boldsymbol{A}_{ei1}\hat{\boldsymbol{x}}_{ei1} + \boldsymbol{\Phi}_{ei1} + \boldsymbol{K}_{ei1}\boldsymbol{C}_{ei1}(\boldsymbol{x}_{ei1} - \hat{\boldsymbol{x}}_{ei1}) \quad (27)$$

where $\hat{\boldsymbol{x}}_{ei1}$ is the estimate of $\boldsymbol{x}_{ei1}$, and the observer gain $\boldsymbol{K}_{ei1}$ can be chosen as

$$\boldsymbol{K}_{ei1} = \left[3\omega_{ei1}, 3\omega_{ei1}^2, \omega_{ei1}^3\right]^T, \quad (28)$$

in which $\omega_{ei1} > 0$ is a design parameter that can be seen as the bandwidth of the observer.

Denote the state estimation error as $\tilde{\boldsymbol{x}}_{ei1} = \boldsymbol{x}_{ei1} - \hat{\boldsymbol{x}}_{ei1} = [\tilde{x}_{i1}, \tilde{x}_{i2}, \tilde{x}_{ei1}]^T$ and the scaled estimation error as $\boldsymbol{\varepsilon}_i = [\varepsilon_{i1}, \varepsilon_{i2}, \varepsilon_{i3}]^T = [\tilde{x}_{i1}, \tilde{x}_{i2}/\omega_{ei1}, \tilde{x}_{ei1}/\omega_{ei1}^2]^T$, thus the dynamics of the scaled estimation error can be described as

$$\dot{\boldsymbol{\varepsilon}}_i = \omega_{ei1}\boldsymbol{A}_{\varepsilon i}\boldsymbol{\varepsilon}_i + \boldsymbol{B}_{\varepsilon i}\frac{h_{ei1}(t)}{\omega_{ei1}^2} \quad (29)$$

where $\boldsymbol{A}_{\varepsilon i} = \begin{bmatrix} -3 & 1 & 0 \\ -3 & 0 & 1 \\ -1 & 0 & 0 \end{bmatrix}$, $\boldsymbol{B}_{\varepsilon i} = \begin{bmatrix} 0 \\ 0 \\ 1 \end{bmatrix}$.

Since the matrix $\boldsymbol{A}_{\varepsilon i}$ is Hurwitz, there exists a symmetric positive definite matrix $\boldsymbol{P}_{i1}$ that satisfies

$$\boldsymbol{A}_{\varepsilon i}^T\boldsymbol{P}_{i1} + \boldsymbol{P}_{i1}\boldsymbol{A}_{\varepsilon i} = -\boldsymbol{I}. \quad (30)$$

Remark 4: It should be noted that the ESOs in (27) are driven by position signals rather than by velocity signals, which can greatly reduce the effect of the measurement noise in the disturbance estimations.

Two linear ESOs which are denoted as DOB12 and DOB22 are constructed to estimate the matched disturbance in HA1 and HA2 respectively.

Based on the last equation of (11), there are two ways of defining an extended state vector:

Case 1: Let $\boldsymbol{x}_{ei2} = [x_{i3}, x_{ei2}]^T = [A_1P_{hi1} - A_2P_{hi2}, q_i]^T$, then an extended state equation is described as

$$\begin{cases} \dot{\boldsymbol{x}}_{ei2} = \boldsymbol{A}_{ei2}\boldsymbol{x}_{ei2} + \boldsymbol{\Phi}_{ei2} + \boldsymbol{\varphi}_{ei2} + \boldsymbol{H}_{ei2} \\ y_{ei2} = \boldsymbol{C}_{ei2}\boldsymbol{x}_{ei2} \end{cases} \quad (31)$$

where $\boldsymbol{A}_{ei2} = \begin{bmatrix} 0 & 1 \\ 0 & 0 \end{bmatrix}$, $\boldsymbol{\Phi}_{ei2} = \begin{bmatrix} f_{hi1}u_i - f_{hi2} \\ 0 \end{bmatrix}$, $\boldsymbol{\varphi}_{ei2} = \begin{bmatrix} -f_{hi3}\hat{\theta}_i \\ 0 \end{bmatrix}$, $\boldsymbol{H}_{ei2} = [-f_{hi3}\tilde{\theta}_i, h_{ei2}(t)]^T$ and $\boldsymbol{C}_{ei2} = [1, 0]$. In which $h_{ei2}(t)$ denotes the change rate of the matched disturbance q_i and it is unknown but bounded.

Case 2: Let $\boldsymbol{x}_{ei2} = [x_{i3}, x_{ei2}]^T = [A_1P_{hi1} - A_2P_{hi2}, q_i - f_{hi3}\tilde{\theta}_i]^T$. The extended state equation has a similar form as (31), and the only difference lies in the expression of $\boldsymbol{H}_{ei2}$, here $\boldsymbol{H}_{ei2} = [0, h_{ei2}(t)]^T$.

Whatever the definition of the extended state we adopt, the constructed ESOs are the same and they are described as

$$\dot{\hat{\boldsymbol{x}}}_{ei2} = \boldsymbol{A}_{ei2}\hat{\boldsymbol{x}}_{ei2} + \boldsymbol{\Phi}_{ei2} + \boldsymbol{\varphi}_{ei2} + \boldsymbol{K}_{ei2}\boldsymbol{C}_{ei2}(\boldsymbol{x}_{ei2} - \hat{\boldsymbol{x}}_{ei2}) \quad (32)$$

where $\hat{\boldsymbol{x}}_{ei2}$ is the estimate of $\boldsymbol{x}_{ei2}$, $\boldsymbol{K}_{ei2} = \left[2\omega_{ei2}, \omega_{ei2}^2\right]^T$ is the observer gain and $\omega_{ei2} > 0$ is the bandwidth of the observer.

Denote the state estimation error as $\tilde{\boldsymbol{x}}_{ei2} = \boldsymbol{x}_{ei2} - \hat{\boldsymbol{x}}_{ei2} = [\tilde{x}_{i3}, \tilde{x}_{ei2}]^T$ and the scaled estimation error as $\boldsymbol{\eta}_i = [\eta_{i1}, \eta_{i2}]^T = \left[\tilde{x}_{i3}, \tilde{x}_{ei2}/\omega_{ei2}\right]^T$. For case 1, the dynamics of the scaled estimation error can be described as

$$\dot{\boldsymbol{\eta}}_i = \omega_{ei2}\boldsymbol{A}_{\eta i}\boldsymbol{\eta}_i + \boldsymbol{B}_{\eta i}\frac{h_{ei2}(t)}{\omega_{ei2}} - \boldsymbol{D}_{\eta i}f_{hi3}\tilde{\theta}_i \quad (33)$$

where $\boldsymbol{A}_{\eta i} = \begin{bmatrix} -2 & 1 \\ -1 & 0 \end{bmatrix}$, $\boldsymbol{B}_{\eta i} = \begin{bmatrix} 0 \\ 1 \end{bmatrix}$ and $\boldsymbol{D}_{\eta i} = \begin{bmatrix} 1 \\ 0 \end{bmatrix}$.

Considering the case 2, the dynamics of the scaled estimation error can be given by

$$\dot{\boldsymbol{\eta}}_i = \omega_{ei2}\boldsymbol{A}_{\eta i}\boldsymbol{\eta}_i + \boldsymbol{B}_{\eta i}\frac{h_{ei2}(t)}{\omega_{ei2}}. \quad (34)$$

Remark 5: The derived observer estimation errors (33) and (34) will facilitate the latter stability analysis to achieve different theoretical results in different conditions.

Since $\boldsymbol{A}_{\eta i}$ is Hurwitz, there exists a symmetric positive definite matrix $\boldsymbol{P}_{i2}$ that satisfies

$$\boldsymbol{A}_{\eta i}^T\boldsymbol{P}_{i2} + \boldsymbol{P}_{i2}\boldsymbol{A}_{\eta i} = -\boldsymbol{I}. \quad (35)$$

C. CONTROLLER DESIGN

To achieve the control objectives, based on the system model (21), a DAFTSC controller is presented in this section. The design procedure of the controller is presented as follows:

Step 1: Denote the reference trajectory as $\boldsymbol{x}_{\mathrm{r}} = [x_{\mathrm{r}1}, x_{\mathrm{r}2}]^T$ and the tracking error of the system (21) is

$$z_1 = [\mathrm{z}_{11}, \mathrm{z}_{12}]^T = \boldsymbol{f}(x_{11}, x_{21}, t) - \boldsymbol{x}_{\mathrm{r}}. \tag{36}$$

Using a virtual control law $\boldsymbol{\alpha}_1 = [\alpha_{11}, \alpha_{12}]^T$ to stabilize $\boldsymbol{f}(x_{12}, x_{22}, t)$ and the error between $\boldsymbol{f}(x_{12}, x_{22}, t)$ and $\boldsymbol{\alpha}_1$ is defined as

$$z_2 = [\mathrm{z}_{21}, \mathrm{z}_{22}]^T = \dot{z}_1 + \boldsymbol{k}_1 z_1 = \boldsymbol{f}(x_{12}, x_{22}, t) - \boldsymbol{\alpha}_1 \tag{37}$$

where $\boldsymbol{\alpha}_1 \triangleq -\boldsymbol{k}_1 z_1 + \dot{\boldsymbol{x}}_{\mathrm{r}}$, in which the feedback gain matrix $\boldsymbol{k}_1 = diag(k_{11}, k_{12})$ is a diagonal positive definite matrix.

Considering (21), (37) and differentiating z_2 with respect to time, we can derive that

$$\begin{aligned}\dot{z}_2 = &-\boldsymbol{M}_1\boldsymbol{f}(x_{11}, x_{21}, t) - \boldsymbol{M}_2\boldsymbol{f}(x_{12}, x_{22}, t) + \bar{\boldsymbol{x}}_3 \\ &+ \boldsymbol{M}_4\boldsymbol{x}_{\mathrm{c}} + \boldsymbol{T}\boldsymbol{H}_{\mathrm{d}} - \dot{\boldsymbol{\alpha}}_1.\end{aligned} \tag{38}$$

Let $\boldsymbol{\alpha}_2 = [\alpha_{21}, \alpha_{22}]^T$ denotes the virtual control law of the state $\bar{\boldsymbol{x}}_3$, and the discrepancy between $\bar{\boldsymbol{x}}_3$ and $\boldsymbol{\alpha}_2$ is defined as

$$z_3 = [\mathrm{z}_{31}, \mathrm{z}_{32}]^T = \bar{\boldsymbol{x}}_3 - \boldsymbol{\alpha}_2. \tag{39}$$

Combining the two-channel mismatched disturbances into a new vector $\boldsymbol{x}_{\mathrm{e}1} = [x_{\mathrm{e}11}, x_{\mathrm{e}21}]^T$. Let $\hat{\boldsymbol{x}}_{\mathrm{e}1} = \left[\hat{x}_{\mathrm{e}11}, \hat{x}_{\mathrm{e}21}\right]^T$ denotes the estimate of $\boldsymbol{x}_{\mathrm{e}1}$, thus the virtual control law $\boldsymbol{\alpha}_2$ can be designed as

$$\begin{aligned}\boldsymbol{\alpha}_2 &= \boldsymbol{\alpha}_{2a} + \boldsymbol{\alpha}_{2s} \\ \boldsymbol{\alpha}_{2a} &= \boldsymbol{M}_1\boldsymbol{f}(x_{11}, x_{21}, t) + \boldsymbol{M}_2\boldsymbol{f}(x_{12}, x_{22}, t) - \boldsymbol{M}_4\boldsymbol{x}_c \\ &\quad -\boldsymbol{T}\hat{x}_{\mathrm{e}1} + \dot{\boldsymbol{\alpha}}_1, \\ \boldsymbol{\alpha}_{2s} &= -\boldsymbol{k}_2 z_2\end{aligned} \tag{40}$$

where $\boldsymbol{\alpha}_{2a}$ is a model compensation term,$\boldsymbol{\alpha}_{2s}$ functions as a nominal stabilizing feedback, and the feedback gain matrix $\boldsymbol{k}_2 = diag(k_{21}, k_{22})$ is a diagonal positive definite matrix.

Substituting (39), (40) into (38), then we have

$$\dot{z}_2 = z_3 + \boldsymbol{T}\boldsymbol{H}_{\mathrm{d}} - T\hat{\boldsymbol{x}}_{\mathrm{e}1} - \boldsymbol{k}_2 z_2. \tag{41}$$

Step 2: Considering (21), (39) and differentiating z_3 with respect to time, we can obtain

$$\dot{z}_3 = \boldsymbol{M}_3\boldsymbol{F}_1\boldsymbol{u} - \boldsymbol{M}_3\boldsymbol{F}_2 - \boldsymbol{M}_3\boldsymbol{F}_3\boldsymbol{\theta} + \boldsymbol{M}_3\boldsymbol{H}_{\mathrm{q}} - \dot{\boldsymbol{\alpha}}_2 \tag{42}$$

and based on (40), the derivative of the virtual control $\boldsymbol{\alpha}_2$ can be calculated by

$$\begin{aligned}\dot{\boldsymbol{\alpha}}_2 &= \dot{\boldsymbol{\alpha}}_{2c} + \dot{\boldsymbol{\alpha}}_{2u} \\ \dot{\boldsymbol{\alpha}}_{2c} &= \frac{\partial\boldsymbol{\alpha}_2}{\partial t} + \frac{\partial\boldsymbol{\alpha}_2}{\partial\boldsymbol{f}(x_{11}, x_{21}, t)}\boldsymbol{f}(x_{12}, x_{22}, t) \\ &\quad + \frac{\partial\boldsymbol{\alpha}_2}{\partial\boldsymbol{f}(x_{12}, x_{22}, t)}[-\boldsymbol{M}_1\boldsymbol{f}(x_{11}, x_{21}, t) \\ &\quad -\boldsymbol{M}_2\boldsymbol{f}(x_{12}, x_{22}, t) + \bar{\boldsymbol{x}}_3 + \boldsymbol{M}_4\boldsymbol{x}_{\mathrm{c}} + \boldsymbol{T}\hat{\boldsymbol{x}}_{\mathrm{e}1}] + \frac{\partial\boldsymbol{\alpha}_2}{\partial\hat{\boldsymbol{x}}_{\mathrm{e}1}}\dot{\hat{\boldsymbol{x}}}_{\mathrm{e}1} \\ \dot{\boldsymbol{\alpha}}_{2u} &= \frac{\partial\boldsymbol{\alpha}_2}{\partial\boldsymbol{f}(x_{12}, x_{22}, t)}\boldsymbol{T}\tilde{\boldsymbol{x}}_{\mathrm{e}1}.\end{aligned} \tag{43}$$

in which $\dot{\boldsymbol{\alpha}}_{2c}$ belongs to the calculable part of $\dot{\boldsymbol{\alpha}}_2$ that can be employed in the controller design, $\boldsymbol{\alpha}_{2u}$ represents the incalculable part that will be adjusted by certain robust feedback control design, and $\tilde{\boldsymbol{x}}_{\mathrm{e}1} = \left[\tilde{x}_{\mathrm{e}11}, \tilde{x}_{\mathrm{e}21}\right]^T = \boldsymbol{x}_{\mathrm{e}1} - \hat{\boldsymbol{x}}_{\mathrm{e}1}$.

Combining the two-channel matched disturbances into a vector $\boldsymbol{x}_{\mathrm{e}2} = [x_{\mathrm{e}12}, x_{\mathrm{e}22}]^T$ and let $\hat{\boldsymbol{x}}_{\mathrm{e}2} = \left[\hat{x}_{\mathrm{e}12}, \hat{x}_{\mathrm{e}22}\right]^T$ denotes the estimate of $\boldsymbol{x}_{\mathrm{e}2}$.

Note that the matrices $\boldsymbol{F}_1$ and $\boldsymbol{M}_3$ are reversible, then based on (42) and (43), the control law $\boldsymbol{u}$ can be designed as

$$\begin{aligned}\boldsymbol{u} &= \boldsymbol{F}_1^{-1}\boldsymbol{M}_3^{-1}(\boldsymbol{u}_{\mathrm{a}} + \boldsymbol{u}_{\mathrm{s}}) \\ \boldsymbol{u}_{\mathrm{a}} &= \boldsymbol{M}_3\boldsymbol{F}_2 + \boldsymbol{M}_3\boldsymbol{F}_3\hat{\boldsymbol{\theta}} - \boldsymbol{M}_3\hat{\boldsymbol{x}}_{\mathrm{e}2} + \dot{\boldsymbol{\alpha}}_{2c} \\ \boldsymbol{u}_{\mathrm{s}} &= -\boldsymbol{k}_3 z_3\end{aligned} \tag{44}$$

where the feedback gain matrix $\boldsymbol{k}_3 = diag(k_{31}, k_{32})$ is a diagonal positive definite matrix. $\boldsymbol{u}_{\mathrm{a}}$ is an adjustable model compensation term through the use of fault parameters online adaptation and disturbance estimation, and $\boldsymbol{u}_{\mathrm{s}}$ is a linear robust control law to help stabilize the closed-loop system.

Denote $\tilde{\boldsymbol{x}}_{\mathrm{e}2} = \left[\tilde{x}_{\mathrm{e}12}, \tilde{x}_{\mathrm{e}22}\right]^T = \boldsymbol{x}_{\mathrm{e}2} - \hat{\boldsymbol{x}}_{\mathrm{e}2}$, then by substituting (44) into (42) we can obtain

$$\begin{aligned}\dot{z}_3 = &-\boldsymbol{M}_3\boldsymbol{F}_3\tilde{\boldsymbol{\theta}} + \boldsymbol{M}_3\boldsymbol{H}_{\mathrm{q}} - \boldsymbol{M}_3\boldsymbol{x}_{\mathrm{e}2} + \boldsymbol{M}_3\tilde{\boldsymbol{x}}_{\mathrm{e}2} \\ &-\dot{\boldsymbol{\alpha}}_{2u} - \boldsymbol{k}_3 z_3.\end{aligned} \tag{45}$$

D. STABILITY ANALYSIS

To facilitate the system stability analysis, some parameter matrices are introduced as follows:

$$\begin{aligned}&\boldsymbol{W}_{\mathrm{e}1} = \begin{bmatrix}\omega_{\mathrm{e}11}\mathbf{I}_3 & \mathbf{0}_3 \\ \mathbf{0}_3 & \omega_{\mathrm{e}21}\mathbf{I}_3\end{bmatrix}, \quad \boldsymbol{W}_{\mathrm{e}2} = \begin{bmatrix}\omega_{\mathrm{e}12}\mathbf{I}_2 & \mathbf{0}_2 \\ \mathbf{0}_2 & \omega_{\mathrm{e}22}\mathbf{I}_2\end{bmatrix}, \\ &\boldsymbol{M}_{\mathrm{e}1} = \begin{bmatrix}\omega_{\mathrm{e}11} & 0 \\ 0 & \omega_{\mathrm{e}21}\end{bmatrix}, \quad \boldsymbol{M}_{\mathrm{e}2} = \begin{bmatrix}\omega_{\mathrm{e}12} & 0 \\ 0 & \omega_{\mathrm{e}22}\end{bmatrix}, \\ &\boldsymbol{N}_1 = \begin{bmatrix}0 & 0 & 1 & 0 & 0 & 0 \\ 0 & 0 & 0 & 0 & 0 & 1\end{bmatrix}, \\ &\boldsymbol{N}_2 = \begin{bmatrix}0 & 1 & 0 & 0 \\ 0 & 0 & 0 & 1\end{bmatrix}.\end{aligned} \tag{46}$$

Theorem 2: Consider the DRHAS (21) with internal leakage faults, constant or slowly-varying disturbances, i.e.,$h_{\mathrm{e}11}(t) = h_{\mathrm{e}21}(t) = 0$, $h_{\mathrm{e}12}(t) = h_{\mathrm{e}22}(t) = 0$, the proposed controller (44) combined with the four constructed disturbance observers (27), (32) and the adaptation function presented by

$$\boldsymbol{\sigma} = -\omega_3\boldsymbol{F}_3^T\boldsymbol{M}_3^T z_3 - \mu_2\boldsymbol{F}_3^T\boldsymbol{D}_\eta^T\boldsymbol{P}_2\boldsymbol{\eta} \tag{47}$$

can guarantee that all the closed-loop system signals are bounded, the fault estimation error, the disturbance estimation error and the system tracking error converge to zero asymptotically if the following matrix $\boldsymbol{\Lambda}$ is positive definite by selecting suitable feedback gain matrices $\boldsymbol{k}_1$, $\boldsymbol{k}_2$, $\boldsymbol{k}_3$ and proper positive design parameters ω_2, ω_3, μ_1 and μ_2.

$$\boldsymbol{\Lambda} = \begin{bmatrix}\boldsymbol{\Lambda}_1 & \boldsymbol{\Lambda}_2 \\ \boldsymbol{\Lambda}_2^T & \boldsymbol{\Lambda}_3\end{bmatrix} \tag{48}$$

where

$$\boldsymbol{\Lambda}_1 = \begin{bmatrix} \boldsymbol{k}_1 & -0.5\boldsymbol{I}_2 & \boldsymbol{0}_2 \\ -0.5\boldsymbol{I}_2 & \omega_2\boldsymbol{k}_2 & -0.5\omega_2\boldsymbol{I}_2 \\ \boldsymbol{0}_2 & -0.5\omega_2\boldsymbol{I}_2 & \omega_3\boldsymbol{k}_3 \end{bmatrix},$$

$$\boldsymbol{\Lambda}_2 = \begin{bmatrix} \boldsymbol{0}_{2\times 6} & \boldsymbol{0}_{2\times 4} \\ -\frac{1}{2}\omega_2\boldsymbol{T}\boldsymbol{M}_{\mathrm{e1}}^2\boldsymbol{N}_1 & \boldsymbol{0}_{2\times 4} \\ \frac{1}{2}\omega_3(\boldsymbol{M}_2-\boldsymbol{k}_1-\boldsymbol{k}_2)\boldsymbol{T}\boldsymbol{M}_{\mathrm{e1}}^2\boldsymbol{N}_1 & -\frac{1}{2}\omega_3\boldsymbol{M}_3\boldsymbol{M}_{\mathrm{e2}}\boldsymbol{N}_2 \end{bmatrix},$$

$$\boldsymbol{\Lambda}_3 = \begin{bmatrix} \frac{1}{2}\mu_1(\boldsymbol{W}_{\mathrm{e1}}-\boldsymbol{I}_6) & \boldsymbol{0}_{6\times 4} \\ \boldsymbol{0}_{4\times 6} & \frac{1}{2}\mu_2(\boldsymbol{W}_{\mathrm{e2}}-\boldsymbol{I}_4) \end{bmatrix}.$$

Proof: Considering the definitions of $x_{ei1} = -d_i/m_{\mathrm{h}i}$, $x_{ei2} = q_i$ and thus the following relations hold:

$$\boldsymbol{H}_{\mathrm{d}} = \boldsymbol{x}_{\mathrm{e1}}, \quad \boldsymbol{H}_{\mathrm{q}} = \boldsymbol{x}_{\mathrm{e2}}. \tag{49}$$

Let $\boldsymbol{\varepsilon} = \left[\boldsymbol{\varepsilon}_1^T, \boldsymbol{\varepsilon}_2^T\right]^T$, then based on (29) and the parameter matrices $\boldsymbol{W}_{\mathrm{e1}}$ and $\boldsymbol{M}_{\mathrm{e1}}$ in (46), we can obtain:

$$\dot{\boldsymbol{\varepsilon}} = \boldsymbol{W}_{\mathrm{e1}}\boldsymbol{A}_\varepsilon\boldsymbol{\varepsilon} + \boldsymbol{B}_\varepsilon(\boldsymbol{M}_{\mathrm{e1}}^{-1})^2\boldsymbol{H}_{\mathrm{e1}} \tag{50}$$

where $\boldsymbol{A}_\varepsilon = \begin{bmatrix} \boldsymbol{A}_{\varepsilon 1} & \boldsymbol{0}_3 \\ \boldsymbol{0}_3 & \boldsymbol{A}_{\varepsilon 2} \end{bmatrix}$, $\boldsymbol{B}_\varepsilon = \begin{bmatrix} \boldsymbol{B}_{\varepsilon 1} & \boldsymbol{0}_{3\times 1} \\ \boldsymbol{0}_{3\times 1} & \boldsymbol{B}_{\varepsilon 2} \end{bmatrix}$ and $\boldsymbol{H}_{\mathrm{e1}} = \begin{bmatrix} h_{\mathrm{e}11} \\ h_{\mathrm{e}21} \end{bmatrix}$.

It is easy to see the matrix $\boldsymbol{A}_\varepsilon$ is Hurwitz, and there exists a symmetric positive definite matrix $\boldsymbol{P}_1$ satisfying the following Lyapunov equation

$$\boldsymbol{A}_\varepsilon^T\boldsymbol{P}_1 + \boldsymbol{P}_1\boldsymbol{A}_\varepsilon = -\boldsymbol{I} \tag{51}$$

where $\boldsymbol{P}_1 = \begin{bmatrix} \boldsymbol{P}_{11} & \boldsymbol{0} \\ \boldsymbol{0} & \boldsymbol{P}_{21} \end{bmatrix}$.

Similarly, let us denote $\boldsymbol{\eta} = [\boldsymbol{\eta}_1^T, \boldsymbol{\eta}_2^T]^T$, then based on (33) and the parameter matrices $\boldsymbol{W}_{\mathrm{e2}}$ and $\boldsymbol{M}_{\mathrm{e2}}$ defined in (46), we can derive

$$\dot{\boldsymbol{\eta}} = \boldsymbol{W}_{\mathrm{e2}}\boldsymbol{A}_\eta\boldsymbol{\eta} + \boldsymbol{B}_\eta\boldsymbol{M}_{\mathrm{e2}}^{-1}\boldsymbol{H}_{\mathrm{e2}} - \boldsymbol{D}_\eta\boldsymbol{F}_3\tilde{\boldsymbol{\theta}} \tag{52}$$

where $\boldsymbol{A}_\eta = \begin{bmatrix} \boldsymbol{A}_{\eta 1} & \boldsymbol{0}_2 \\ \boldsymbol{0}_2 & \boldsymbol{A}_{\eta 2} \end{bmatrix}$, $\boldsymbol{B}_\eta = \begin{bmatrix} \boldsymbol{B}_{\eta 1} & \boldsymbol{0}_{2\times 1} \\ \boldsymbol{0}_{2\times 1} & \boldsymbol{B}_{\eta 2} \end{bmatrix}$, $\boldsymbol{H}_{\mathrm{e2}} = \begin{bmatrix} h_{\mathrm{e}12} \\ h_{\mathrm{e}22} \end{bmatrix}$ and $\boldsymbol{D}_\eta = \begin{bmatrix} \boldsymbol{D}_{\eta 1} & \boldsymbol{0}_{2\times 1} \\ \boldsymbol{0}_{2\times 1} & \boldsymbol{D}_{\eta 2} \end{bmatrix}$.

Since the matrix $\boldsymbol{A}_\eta$ is Hurwitz, there exists a symmetric positive definite matrix $\boldsymbol{P}_2$ that satisfies the following Lyapunov equation

$$\boldsymbol{A}_\eta^T\boldsymbol{P}_2 + \boldsymbol{P}_2\boldsymbol{A}_\eta = -\boldsymbol{I} \tag{53}$$

where $\boldsymbol{P}_2 = \begin{bmatrix} \boldsymbol{P}_{12} & \boldsymbol{0} \\ \boldsymbol{0} & \boldsymbol{P}_{22} \end{bmatrix}$.

Considering the definitions of $\tilde{\boldsymbol{x}}_{\mathrm{e1}}$, $\tilde{\boldsymbol{x}}_{\mathrm{e2}}$, $\tilde{x}_{ei1}$, $\tilde{x}_{ei2}$, $\boldsymbol{\varepsilon}$ and $\boldsymbol{\eta}$, and by introducing four parameter matrices $\boldsymbol{M}_{\mathrm{e1}}$, $\boldsymbol{M}_{\mathrm{e2}}$, $\boldsymbol{N}_1$ and $\boldsymbol{N}_2$, we can obtain

$$\tilde{\boldsymbol{x}}_{\mathrm{e1}} = \boldsymbol{M}_{\mathrm{e1}}^2\boldsymbol{N}_1\boldsymbol{\varepsilon}, \quad \tilde{\boldsymbol{x}}_{\mathrm{e2}} = \boldsymbol{M}_{\mathrm{e2}}\boldsymbol{N}_2\boldsymbol{\eta} \tag{54}$$

Define a Lyapunov function as

$$V = \frac{1}{2}\boldsymbol{z}_1^T\boldsymbol{z}_1 + \frac{1}{2}\omega_2\boldsymbol{z}_2^T\boldsymbol{z}_2 + \frac{1}{2}\omega_3\boldsymbol{z}_3^T\boldsymbol{z}_3 + \frac{1}{2}\mu_1\boldsymbol{\varepsilon}^T\boldsymbol{P}_1\boldsymbol{\varepsilon} + \frac{1}{2}\mu_2\boldsymbol{\eta}^T\boldsymbol{P}_2\boldsymbol{\eta} + \frac{1}{2}\tilde{\boldsymbol{\theta}}^T\boldsymbol{\Gamma}^{-1}\tilde{\boldsymbol{\theta}}. \tag{55}$$

Then, the derivative of (55) can be described as

$$\dot{V} = \boldsymbol{z}_1^T\dot{\boldsymbol{z}}_1 + \omega_2\boldsymbol{z}_2^T\dot{\boldsymbol{z}}_2 + \omega_3\boldsymbol{z}_3^T\dot{\boldsymbol{z}}_3 + \frac{1}{2}\mu_1\dot{\boldsymbol{\varepsilon}}^T\boldsymbol{P}_1\boldsymbol{\varepsilon} + \frac{1}{2}\mu_1\boldsymbol{\varepsilon}^T\boldsymbol{P}_1\dot{\boldsymbol{\varepsilon}} + \frac{1}{2}\mu_2\dot{\boldsymbol{\eta}}^T\boldsymbol{P}_2\boldsymbol{\eta} + \frac{1}{2}\mu_2\boldsymbol{\eta}^T\boldsymbol{P}_2\dot{\boldsymbol{\eta}} - \dot{\tilde{\boldsymbol{\theta}}}^T\boldsymbol{\Gamma}^{-1}\tilde{\boldsymbol{\theta}}. \tag{56}$$

According to the definitions of $\boldsymbol{W}_{\mathrm{e1}}$ and $\boldsymbol{W}_{\mathrm{e2}}$ in (46), we have

$$\boldsymbol{W}_{\mathrm{e1}} = \boldsymbol{W}_{\mathrm{e1}}^T, \quad \boldsymbol{W}_{\mathrm{e1}}^T\boldsymbol{P}_1 = \boldsymbol{P}_1\boldsymbol{W}_{\mathrm{e1}}, \ \boldsymbol{W}_{\mathrm{e1}}\boldsymbol{A}_\varepsilon = \boldsymbol{A}_\varepsilon\boldsymbol{W}_{\mathrm{e1}}, \tag{57}$$

$$\boldsymbol{W}_{\mathrm{e2}} = \boldsymbol{W}_{\mathrm{e2}}^T, \quad \boldsymbol{W}_{\mathrm{e2}}^T\boldsymbol{P}_2 = \boldsymbol{P}_2\boldsymbol{W}_{\mathrm{e2}}, \ \boldsymbol{W}_{\mathrm{e2}}\boldsymbol{A}_\eta = \boldsymbol{A}_\eta\boldsymbol{W}_{\mathrm{e2}}. \tag{58}$$

Then, noting (50), (51) and (57), we can derive

$$\frac{1}{2}\mu_1\dot{\boldsymbol{\varepsilon}}^T\boldsymbol{P}_1\boldsymbol{\varepsilon} + \frac{1}{2}\mu_1\boldsymbol{\varepsilon}^T\boldsymbol{P}_1\dot{\boldsymbol{\varepsilon}} = -\frac{1}{2}\mu_1\boldsymbol{\varepsilon}^T\boldsymbol{W}_{\mathrm{e1}}\boldsymbol{\varepsilon} + \mu_1\boldsymbol{\varepsilon}^T\boldsymbol{P}_1\boldsymbol{B}_\varepsilon(\boldsymbol{M}_{\mathrm{e1}}^{-1})^2\boldsymbol{H}_{\mathrm{e1}}. \tag{59}$$

Similarly, based on (52), (53) and (58), we have

$$\frac{1}{2}\mu_2\dot{\boldsymbol{\eta}}^T\boldsymbol{P}_2\boldsymbol{\eta} + \frac{1}{2}\mu_2\boldsymbol{\eta}^T\boldsymbol{P}_2\dot{\boldsymbol{\eta}} = -\frac{1}{2}\mu_2\boldsymbol{\eta}^T\boldsymbol{W}_{\mathrm{e2}}\boldsymbol{\eta} + \mu_2\boldsymbol{\eta}^T\boldsymbol{P}_2\boldsymbol{B}_\eta\boldsymbol{M}_{\mathrm{e2}}^{-1}\boldsymbol{H}_{\mathrm{e2}} - \mu_2\tilde{\boldsymbol{\theta}}^T\boldsymbol{F}_3^T\boldsymbol{D}_\eta^T\boldsymbol{P}_2\boldsymbol{\eta}. \tag{60}$$

Substituting (37), (41), (45), (59) and (60) into (56), and note that $h_{\mathrm{e}11}(t) = h_{\mathrm{e}21}(t) = 0$, $h_{\mathrm{e}12}(t) = h_{\mathrm{e}22}(t) = 0$, i.e. $\boldsymbol{H}_{\mathrm{e1}} = \boldsymbol{0}$, $\boldsymbol{H}_{\mathrm{e2}} = \boldsymbol{0}$, thus we can obtain

$$\begin{aligned} \dot{V} = {} & \boldsymbol{z}_1^T(-\boldsymbol{k}_1\boldsymbol{z}_1 + \boldsymbol{z}_2) + \omega_2\boldsymbol{z}_2^T(\boldsymbol{z}_3 + \boldsymbol{T}\boldsymbol{H}_{\mathrm{d}} - \boldsymbol{T}\hat{\boldsymbol{x}}_{\mathrm{e1}} - \boldsymbol{k}_2\boldsymbol{z}_2) \\ & + \omega_3\boldsymbol{z}_3^T(\boldsymbol{M}_3\boldsymbol{H}_{\mathrm{q}} - \boldsymbol{M}_3\boldsymbol{x}_{\mathrm{e2}} + \boldsymbol{M}_3\tilde{\boldsymbol{x}}_{\mathrm{e2}} - \dot{\boldsymbol{\alpha}}_{2u} - \boldsymbol{k}_3\boldsymbol{z}_3) \\ & - \frac{1}{2}\mu_1\boldsymbol{\varepsilon}^T\boldsymbol{W}_{\mathrm{e1}}\boldsymbol{\varepsilon} - \frac{1}{2}\mu_2\boldsymbol{\eta}^T\boldsymbol{W}_{\mathrm{e2}}\boldsymbol{\eta} - \omega_3\boldsymbol{z}_3^T\boldsymbol{M}_3\boldsymbol{F}_3\tilde{\boldsymbol{\theta}} \\ & - \mu_2\tilde{\boldsymbol{\theta}}^T\boldsymbol{F}_3^T\boldsymbol{D}_\eta^T\boldsymbol{P}_2\boldsymbol{\eta} - \dot{\tilde{\boldsymbol{\theta}}}^T\boldsymbol{\Gamma}^{-1}\tilde{\boldsymbol{\theta}}. \end{aligned} \tag{61}$$

Then, substituting (43), (49), (54) and the fault adaptation law (22), (47) into (61), we have

$$\begin{aligned} \dot{V} = {} & -\boldsymbol{z}_1^T\boldsymbol{k}_1\boldsymbol{z}_1 + \boldsymbol{z}_1^T\boldsymbol{z}_2 + \omega_2\boldsymbol{z}_2^T\boldsymbol{z}_3 - \omega_2\boldsymbol{z}_2^T\boldsymbol{k}_2\boldsymbol{z}_2 - \omega_3\boldsymbol{z}_3^T\boldsymbol{k}_3\boldsymbol{z}_3 \\ & + \omega_2\boldsymbol{z}_2^T\boldsymbol{T}\boldsymbol{M}_{\mathrm{e1}}^2\boldsymbol{N}_1\boldsymbol{\varepsilon} + \omega_3\boldsymbol{z}_3^T\boldsymbol{M}_3\boldsymbol{M}_{\mathrm{e2}}\boldsymbol{N}_2\boldsymbol{\eta} \\ & - \omega_3\boldsymbol{z}_3^T(\boldsymbol{M}_2-\boldsymbol{k}_1-\boldsymbol{k}_2)\boldsymbol{T}\boldsymbol{M}_{\mathrm{e1}}^2\boldsymbol{N}_1\boldsymbol{\varepsilon} \\ & - \frac{1}{2}\mu_1\boldsymbol{\varepsilon}^T(\boldsymbol{W}_{\mathrm{e1}}-\boldsymbol{I})\boldsymbol{\varepsilon} - \frac{1}{2}\mu_2\boldsymbol{\eta}^T(\boldsymbol{W}_{\mathrm{e2}}-\boldsymbol{I})\boldsymbol{\eta} \\ & - \frac{1}{2}\mu_1\boldsymbol{\varepsilon}^T\boldsymbol{\varepsilon} - \frac{1}{2}\mu_2\boldsymbol{\eta}^T\boldsymbol{\eta}. \end{aligned} \tag{62}$$

Denote $\boldsymbol{Z} = [\boldsymbol{z}_1^T, \boldsymbol{z}_2^T, \boldsymbol{z}_3^T, \boldsymbol{\varepsilon}^T, \boldsymbol{\eta}^T]^T$. Since the matrix $\boldsymbol{\Lambda}$ in (48) is positive definite, we can obtain

$$\begin{aligned} \dot{V} & \le -\boldsymbol{Z}^T\boldsymbol{\Lambda}\boldsymbol{Z} \\ & \le -\lambda_{\min}(\boldsymbol{\Lambda})(\boldsymbol{z}_1^T\boldsymbol{z}_1 + \boldsymbol{z}_2^T\boldsymbol{z}_2 + \boldsymbol{z}_3^T\boldsymbol{z}_3 + \boldsymbol{\varepsilon}^T\boldsymbol{\varepsilon} + \boldsymbol{\eta}^T\boldsymbol{\eta}) \triangleq -W. \end{aligned} \tag{63}$$

where W is a positive function. Therefore, $V \in L_\infty$, $W \in L_2$ and $\boldsymbol{z}_1$, $\boldsymbol{z}_2$, $\boldsymbol{z}_3$, $\boldsymbol{\varepsilon}$, $\boldsymbol{\eta}$ and $\tilde{\boldsymbol{\theta}}$ are bounded. Since $\boldsymbol{x}_{\mathrm{r}}$ is C^3 continuous and bounded, based on (36), (37) and the definition of $\boldsymbol{\alpha}_1$, it can be derived that $\boldsymbol{f}(x_{11}, x_{21}, t)$, $\boldsymbol{f}(x_{12}, x_{22}, t)$, $\dot{\boldsymbol{z}}_1$ and $\dot{\boldsymbol{\alpha}}_1$ are bounded. Since y_1 is bounded, the coupling term $\boldsymbol{x}_{\mathrm{c}}$ is bounded. According to Assumption 1 and 2, it can be inferred that the states $\boldsymbol{x}$, the extended states $\boldsymbol{x}_{ei1}, \boldsymbol{x}_{ei2}$ and their estimates $\hat{\boldsymbol{x}}_{ei1}, \hat{\boldsymbol{x}}_{ei2}$ are bounded. Therefore,

$\hat{\boldsymbol{x}}_{ei}$ and its time derivative are bounded. Then, noting (39) and (40), it is easy to derive that $\boldsymbol{\alpha}_2$ and $\bar{\boldsymbol{x}}_3$ are bounded. Then, according to (43), $\dot{\boldsymbol{\alpha}}_2$ is bounded. Moreover, noting Assumption 2 and (44), it can be inferred that the system control input $\boldsymbol{u}$ is bounded. In conclusion, all signals in the closed-loop system are bounded. From (29), (33), (37), (41) and (45), it can be inferred that $\dot{W}$ is bounded. Thus W is uniformly continuous. By applying Barbalat's lemma [34], it can be obtained that $W \to 0$ as $t \to \infty$, which leads to the results of Theorem 2.

Theorem 3: For the DRHAS (21) subject to internal leakage faults, uncertain time-varying disturbances, i.e., $h_{e11}(t) \neq 0, h_{e21}(t) \neq 0, h_{e12}(t) \neq 0$ and $h_{e22}(t) \neq 0$, the proposed controller (44) combined with the four disturbance observers (27), (32) can guarantee that all the signals in the closed-loop system are bounded and the following Lyapunov function V

$$V = \frac{1}{2}z_1^T z_1 + \frac{1}{2}\omega_2 z_2^T z_2 + \frac{1}{2}\omega_3 z_3^T z_3 + \frac{1}{2}\mu_1 \boldsymbol{\varepsilon}^T \boldsymbol{P}_1 \boldsymbol{\varepsilon} + \frac{1}{2}\mu_2 \boldsymbol{\eta}^T \boldsymbol{P}_2 \boldsymbol{\eta} \quad (64)$$

is bounded by

$$V \leq \exp(-\lambda t)V(0) + \frac{\xi}{\lambda}[1 - \exp(-\lambda t)] \quad (65)$$

where

$$\xi = \frac{\mu_1}{2}\left(\left\|\boldsymbol{P}_1 \boldsymbol{B}_\varepsilon (\boldsymbol{M}_{e1}^{-1})^2\right\| \|\boldsymbol{H}_{e1}\|_{\max}\right)^2 + \frac{\mu_2}{2}\left(\left\|\boldsymbol{P}_2 \boldsymbol{B}_\eta \boldsymbol{M}_{e2}^{-1}\right\| \|\boldsymbol{H}_{e2}\|_{\max}\right)^2$$

$\lambda = 2\lambda_{\min}(\boldsymbol{\Lambda}) \min\{\lambda_1, 1/\mu_1\lambda_{\max}(\boldsymbol{P}_1), 1/\mu_2\lambda_{\max}(\boldsymbol{P}_2)\}$, and $\lambda_1 = \min\{1, 1/\omega_2, 1/\omega_3\}$.

Proof: Let us consider the definitions $x_{ei1} = -d_i/m_{hi}$, $x_{ei2} = q_i - f_{hi3}\tilde{\theta}$ in this case and then we have

$$\boldsymbol{H}_d = \boldsymbol{x}_{e1}, \quad \boldsymbol{H}_q - \boldsymbol{F}_3\tilde{\boldsymbol{\theta}} = \boldsymbol{x}_{e2}. \quad (66)$$

Let $\boldsymbol{\eta} = [\boldsymbol{\eta}_1^T, \boldsymbol{\eta}_2^T]^T$,according to (34) and the definitions in (46), we can obtain

$$\dot{\boldsymbol{\eta}} = \boldsymbol{W}_{e2}\boldsymbol{A}_\eta \boldsymbol{\eta} + \boldsymbol{B}_\eta \boldsymbol{M}_{e2}^{-1}\boldsymbol{H}_{e2}. \quad (67)$$

Then from (53), (58) and (67), it can be derived that

$$(\frac{1}{2}\mu_2 \boldsymbol{\eta}^T \boldsymbol{P}_2 \boldsymbol{\eta})' = -\frac{1}{2}\mu_2 \boldsymbol{\eta}^T \boldsymbol{W}_{e2}\boldsymbol{\eta} + \mu_2 \boldsymbol{\eta}^T \boldsymbol{P}_2 \boldsymbol{B}_\eta \boldsymbol{M}_{e2}^{-1}\boldsymbol{H}_{e2}. \quad (68)$$

A Lyapunov function V is defined as (64). Substituting (37), (41), (43), (45), (54), (59), (66) and (68) into (64), the time derivative of V can be expressed by

$$\begin{aligned}\dot{V} \leq\ & -z_1^T \boldsymbol{k}_1 z_1 + z_1^T z_2 + \omega_2 z_2^T z_3 - \omega_2 z_2^T \boldsymbol{k}_2 z_2 - \omega_3 z_3^T \boldsymbol{k}_3 z_3 \\ & + \omega_2 z_2^T \boldsymbol{T}\boldsymbol{M}_{e1}^2 \boldsymbol{N}_1 \boldsymbol{\varepsilon} + \omega_3 z_3^T \boldsymbol{M}_3 \boldsymbol{M}_{e2} \boldsymbol{N}_2 \boldsymbol{\eta} \\ & - \omega_3 z_3^T (\boldsymbol{M}_2 - \boldsymbol{k}_1 - \boldsymbol{k}_2)\boldsymbol{T}\boldsymbol{M}_{e1}^2 \boldsymbol{N}_1 \boldsymbol{\varepsilon} \\ & - \frac{1}{2}\mu_1 \boldsymbol{\varepsilon}^T (\boldsymbol{W}_{e1} - \boldsymbol{I})\boldsymbol{\varepsilon} - \frac{1}{2}\mu_2 \boldsymbol{\eta}^T (\boldsymbol{W}_{e2} - \boldsymbol{I})\boldsymbol{\eta} \\ & + \mu_1 \boldsymbol{\varepsilon}^T \boldsymbol{P}_1 \boldsymbol{B}_\varepsilon (\boldsymbol{M}_{e1}^{-1})^2 \boldsymbol{H}_{e1} - \frac{1}{2}\mu_1 \|\boldsymbol{\varepsilon}\|^2 \\ & + \mu_2 \boldsymbol{\eta}^T \boldsymbol{P}_2 \boldsymbol{B}_\eta \boldsymbol{M}_{e2}^{-1}\boldsymbol{H}_{e2} - \frac{1}{2}\mu_2 \|\boldsymbol{\eta}\|^2. \end{aligned} \quad (69)$$

Based on Young's inequality [35], the following inequalities can be derived:

$$\begin{aligned}&\mu_1 \boldsymbol{\varepsilon}^T \boldsymbol{P}_1 \boldsymbol{B}_\varepsilon (\boldsymbol{M}_{e1}^{-1})^2 \boldsymbol{H}_{e1} \\ &\quad \leq \mu_1 \|\boldsymbol{\varepsilon}\| \left\|\boldsymbol{P}_1 \boldsymbol{B}_\varepsilon (\boldsymbol{M}_{e1}^{-1})^2\right\| \|\boldsymbol{H}_{e1}\|_{\max} \\ &\quad \leq \frac{\mu_1}{2}\|\boldsymbol{\varepsilon}\|^2 + \frac{\mu_1}{2}\left(\left\|\boldsymbol{P}_1 \boldsymbol{B}_\varepsilon (\boldsymbol{M}_{e1}^{-1})^2\right\| \|\boldsymbol{H}_{e1}\|_{\max}\right)^2, \end{aligned} \quad (70)$$

$$\begin{aligned}&\mu_2 \boldsymbol{\eta}^T \boldsymbol{P}_2 \boldsymbol{B}_\eta \boldsymbol{M}_{e2}^{-1} \boldsymbol{H}_{e2} \\ &\quad \leq \mu_2 \|\boldsymbol{\eta}\| \left\|\boldsymbol{P}_2 \boldsymbol{B}_\eta \boldsymbol{M}_{e2}^{-1}\right\| \|\boldsymbol{H}_{e2}\|_{\max} \\ &\quad \leq \frac{\mu_2}{2}\|\boldsymbol{\eta}\|^2 + \frac{\mu_2}{2}\left(\left\|\boldsymbol{P}_2 \boldsymbol{B}_\eta \boldsymbol{M}_{e2}^{-1}\right\| \|\boldsymbol{H}_{e2}\|_{\max}\right)^2. \end{aligned} \quad (71)$$

Substituting (70) and (71) into (69), we have

$$\begin{aligned}\dot{V} \leq\ & -z_1^T \boldsymbol{k}_1 z_1 + z_1^T z_2 + \omega_2 z_2^T z_3 - \omega_2 z_2^T \boldsymbol{k}_2 z_2 - \omega_3 z_3^T \boldsymbol{k}_3 z_3 \\ & + \omega_2 z_2^T \boldsymbol{T}\boldsymbol{M}_{e1}^2 \boldsymbol{N}_1 \boldsymbol{\varepsilon} + \omega_3 z_3^T \boldsymbol{M}_3 \boldsymbol{M}_{e2} \boldsymbol{N}_2 \boldsymbol{\eta} \\ & - \omega_3 z_3^T (\boldsymbol{M}_2 - \boldsymbol{k}_1 - \boldsymbol{k}_2)\boldsymbol{T}\boldsymbol{M}_{e1}^2 \boldsymbol{N}_1 \boldsymbol{\varepsilon} \\ & - \frac{1}{2}\mu_1 \boldsymbol{\varepsilon}^T (\boldsymbol{W}_{e1} - \boldsymbol{I})\boldsymbol{\varepsilon} - \frac{1}{2}\mu_2 \boldsymbol{\eta}^T (\boldsymbol{W}_{e2} - \boldsymbol{I})\boldsymbol{\eta} \\ & + \frac{\mu_1}{2}\left(\left\|\boldsymbol{P}_1 \boldsymbol{B}_\varepsilon (\boldsymbol{M}_{e1}^{-1})^2\right\| \|\boldsymbol{H}_{e1}\|_{\max}\right)^2 \\ & + \frac{\mu_2}{2}\left(\left\|\boldsymbol{P}_2 \boldsymbol{B}_\eta \boldsymbol{M}_{e2}^{-1}\right\| \|\boldsymbol{H}_{e2}\|_{\max}\right)^2 \\ \leq\ & -\boldsymbol{Z}^T \Lambda \boldsymbol{Z} + \xi. \end{aligned} \quad (72)$$

Since the matrix $\boldsymbol{\Lambda}$ is positive definite, then we have

$$\begin{aligned}\dot{V} \leq\ & -\lambda_{\min}(\boldsymbol{\Lambda})(z_1^T z_1 + z_2^T z_2 + z_3^T z_3 + \boldsymbol{\varepsilon}^T \boldsymbol{\varepsilon} + \boldsymbol{\eta}^T \boldsymbol{\eta}) + \xi \\ \leq\ & -\lambda_{\min}(\boldsymbol{\Lambda})[2\lambda_1(\frac{1}{2}z_1^T z_1 + \frac{1}{2}\omega_2 z_2^T z_2 + \frac{1}{2}\omega_3 z_3^T z_3) \\ & + \frac{2}{\mu_1 \lambda_{\max}(\boldsymbol{P}_1)}(\frac{1}{2}\mu_1 \boldsymbol{\varepsilon}^T \boldsymbol{P}_1 \boldsymbol{\varepsilon}) + \frac{2}{\mu_2 \lambda_{\max}(\boldsymbol{P}_2)}(\frac{1}{2}\mu_2 \boldsymbol{\eta}^T \boldsymbol{P}_2 \boldsymbol{\eta})] \\ & + \xi \leq -\lambda V + \xi. \end{aligned} \quad (73)$$

which leads to the results shown in Theorem 3.

Remark 6: Noting (65), a prescribed tracking performance can be achieved, i.e., the transient response and steady-state error of the system can be adjusted via several controller parameters to fulfill the design requirements. Specifically, the transient response can be speeded up by

increasing λ and the steady-state tracking error ξ/λ can be made arbitrarily small by increasing λ or decreasing ξ. For example, the value of λ can be increased by selecting suitable feedback gain matrices $\boldsymbol{k}_1$, $\boldsymbol{k}_2$, $\boldsymbol{k}_3$ to increase the value of $\lambda_{\min}(\boldsymbol{\Lambda})$ on the premise that the matrix $\boldsymbol{\Lambda}$ is positive definite, and the value of ξ can be reduced by improving the observer bandwidths ω_{e11}, ω_{e12}, ω_{e21} and ω_{e22}.

IV. SIMULATION RESULTS

A model of a DRHAS was established in the MATLAB/Simulink environment. The parameters of the model are listed in Table 1.

To evaluate the control performance of the proposed algorithm in the face of internal leakage faults, large disturbances and force fighting problem, the following four algorithms

TABLE 1. Parameters of the simulation model [29].

Parameter	Description	Value
P_{s1} , P_{s2}	Oil supply pressure	28(Mpa)
P_{r1} , P_{r2}	Oil reservoir pressure	0(Mpa)
k_{u1} , k_{u2}	Servovalve gain	3.04×10^{-3} (m / A)
k_q	Flow rate gain	7.5×10^{-5} (m^2 / s / $pa^{1/2}$)
m_{h1} , m_{h2}	Piston mass	55(Kg)
A_1 , A_2	Piston area	1.47×10^{-3} (m^2)
β_e	Effective oil bulk modulus	800(Mpa)
B_{h1} , B_{h2}	Damping coefficient	1×10^{4} (Ns / m)
V_{10} , V_{20}	Initial volume	0.735×10^{-4} (m^3)
C_{i1} , C_{i2}	Normal internal leakage coefficient	1×10^{-12} (m^3 / s / pa)
K_{h1} , K_{h2}	Connection stiffness	1×10^{8} (N / m)
r_d	Radial distance	0.15(m)
J_d	Moment of inertia	13.5(Kgm^2)
β_d	Damping coefficient	51.75(Nms)
K_d	Elastic load coefficient	9.14×10^{5} (N / m)

with similar control structure (shown as Figure 2) are used for comparison.

1) DAFTSC: The parameters of the proposed control algorithm are chosen as: $\boldsymbol{k}_1 = \boldsymbol{k}_2 = \boldsymbol{k}_3 = diag(1000, 1000)$, $\omega_2 = 1\times10^{-6}$, $\omega_3 = 1\times10^{-12}$, $\mu_1 = 1\times10^{14}$, $\mu_2 = 1\times10^{10}$. The parameters for designing the reference trajectory x_{r1} in (17) are chosen as: k_1=k_2 = 300.The gains of the four ESOs are chosen as: $\omega_{e11} = \omega_{e21} = 250$, $\omega_{e12} = \omega_{e22} = 500$. The upper and lower bounds of the faults are:$\theta_{1\max} = \theta_{2\max} = 5\times10^{-6}$, $\theta_{1\min} = \theta_{2\min} = 0$, and the fault adaptation rates are chosen as: $\Gamma_1 = \Gamma_2 = 1\times10^{-35}$.

2) Adaptive Fault-tolerant Synchronization Control (AFTSC): This control algorithm is similar to the proposed DAFTSC algorithm but without consideration of disturbance compensation. To achieve a fair comparison between these two algorithms, the parameters of the control algorithm, the parameters for the reference trajectory x_{r1} design and the fault adaptation rates are the same as those chosen by DAFTSC.

3) Disturbance-estimation based Synchronization Control (DSC): This control algorithm is similar to DAFTSC but without fault tolerance capability, and the value of the parameter $\hat{\theta}_i$ in observer (32) is set to zero by default. The other parameters setting in the algorithm are the same as those in DAFTSC.

4) Robust Synchronization Control (RSC): This algorithm has the same control structure as the other three ones. However, only robust feedback control terms are employed to handle the disturbances and faults in the DRHAS, and the feedback control gains are the same as those chosen by DAFTSC.

In addition, $\theta_r = \arctan(0.2\sin(2\pi t))[1-\exp(-0.1t^3)]$ rad which fulfills the Assumption 3 is employed as the reference trajectory of the system. An elastic load $F_L = K_d x_d$ is used to simulate the air loads acting on the control surface. Consider the following fault scenario: at $t = 10s$, an internal leakage fault with $C_{t1} = 1\times10^{-7}(m^3/s/pa)$ occurs in HA1 and an internal leakage fault with $C_{t2} = 5\times10^{-7}(m^3/s/pa)$ occurs in HA2.

To test the control performance of each algorithm under large disturbance condition, two types of disturbances are inserted. The unmatched disturbances, i.e., the lumped disturbances d_1 and d_2 in two HA channels are set as: $d_1 = 100\sin(2\pi t)$, $d_2 = 400\sin(2\pi t)$. Moreover, two input disturbances which have the similar form as the system reference trajectory have been added to the system by modifying the control inputs [36], i.e., $\Delta u_1 = \Delta u_2 = 1.5\arctan(0.2\sin(2\pi t))[1-\exp(-0.1t^3)]$. These disturbances are employed to simulate the matched disturbances which can greatly affect the dynamics of the system. From (3)-(6) and (11), we can further derive the expressions of the matched disturbances in both HAs as

$$q_1 = \frac{A_1\beta_e}{V_{h11}}k_q k_{u1}R_{h11}\Delta u_1 + \frac{A_2\beta_e}{V_{h12}}k_q k_{u1}R_{h12}\Delta u_1, \quad (74)$$

$$q_2 = \frac{A_1\beta_e}{V_{h21}}k_q k_{u2}R_{h21}\Delta u_2 + \frac{A_2\beta_e}{V_{h22}}k_q k_{u2}R_{h22}\Delta u_2. \quad (75)$$

Remark 7: According to equations (74), (75), (7) and (8), it can be observed that the matched disturbances q_1 and q_2 inserted in this simulation test vary with the changes of the chamber pressures P_{hi1} and P_{hi2}. Since the internal leakage faults can cause significant changes in chamber pressures of the HAs, the amplitudes of the matched disturbances will change after the occurrence of the faults.

Three performance indexes [36], i.e., the maximum, the average and the standard deviation of the position tracking errors (M_e, μ_e, σ_e) are used to evaluate the steady-state position tracking performance before and after fault occurrence. Similarly, the maximum, the average and the standard deviation of the fighting force between HA channels (M_f, μ_f, σ_f) are introduced to assess the synchronization performance of each algorithm before and after fault occurrence. Moreover, the indexes M_e and M_f are used to investigate the fault-tolerant ability of each algorithm during the fault transient time. The steady-state indexes are calculated from the data of the last three cycles of the corresponding steady-state time period, and the fault transient performance indexes are calculated based on all the data of the transient time period.

Figure 3 compares the position tracking performance of the four algorithms, and the corresponding performance indexes are summarized in Table 2. The curves of the fighting force between HA channels under the control of four algorithms are shown in Figure 4 and the specific indexes for the measurement of the system synchronization performance are listed in the Table 3.

TABLE 2. Indexes for measurement of position tracking performance for four algorithms.

Algorithms	Steady state before fault occurrence $t \in [5s, 10s)$			Fault Transient $t \in [10s, 11s)$	Steady state after fault occurrence $t \in [25s, 30s)$		
	M_e (rad)	μ_e (rad)	σ_e (rad)	M_e (rad)	M_e (rad)	μ_e (rad)	σ_e (rad)
RSC	0.0068	0.0033	0.0022	0.0076	0.0076	0.0050	0.0021
DSC	6.4248e-004	9.3518e-005	9.9560e-005	0.0013	0.0013	6.4505e-004	9.9560e-005
AFTSC	0.0017	7.4245e-004	5.3790e-004	0.0059	0.0014	4.7411e-004	4.5464e-004
DAFTSC	6.4987e-004	9.5390e-005	1.0113e-004	9.1860e-004	4.0139e-004	5.2185e-005	5.1044e-005

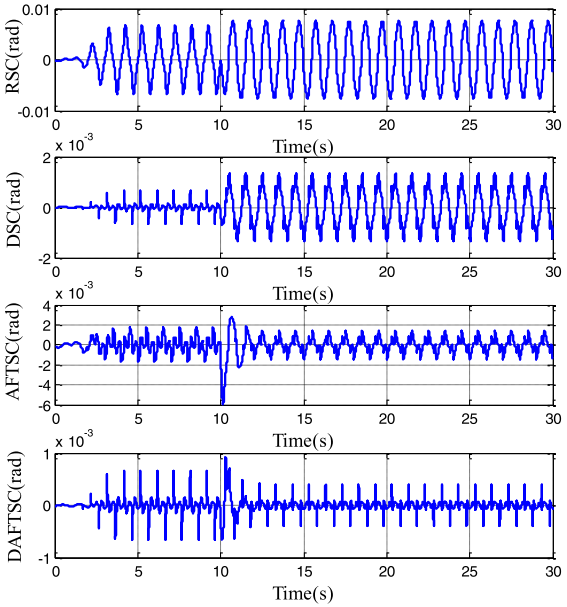

FIGURE 3. Position tracking error.

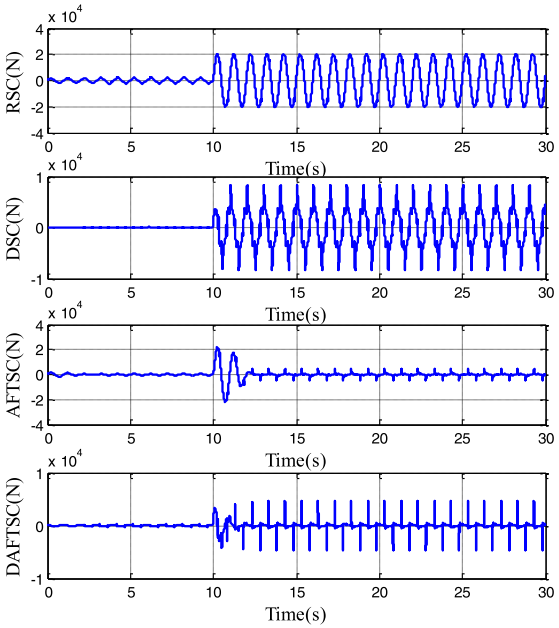

FIGURE 4. Fighting force between HA channels.

From the simulation results, it can be observed that under normal condition, disturbances is the main factor affecting the position tracking performance of the system and the two algorithms with disturbance estimation and compensation, namely, the proposed algorithm and the DSC algorithm can achieve better positon tracking accuracy than the other algorithms. In addition, by comparing the index of the standard deviation σ_e, it can be found that the position tracking accuracy of the algorithm with disturbance estimation and compensation fluctuates less than the other algorithms. Furthermore, influenced by the unequal disturbances, the fighting force between two HA channels is enlarged. Even with the same synchronization control mechanism, the synchronization performance of some algorithms can decrease dramatically. For example, the maximum fighting force for RSC can reach 2.6338e+003 N. In contrast, the maximum fighting force can be reduced to 273.4514N by the proposed DAFTSC algorithm due to the use of disturbance estimation and compensation.

During the fault-transient time, the position tracking performance degradation can be further aggravated by large disturbances, especially for the system without disturbance compensation. As shown in Figure 3 and Table 2, under the same fault condition, the maximum position tracking error for RSC can reach 0.0076 rad, larger than the other three algorithms. This means that the algorithm with only robust feedback control design cannot accommodate the faults and large disturbances anymore. In comparison, by utilizing the disturbance compensation design, the algorithms DAFTSC and DSC can suppress the deterioration in position tracking performance more effectively than the other algorithms.

Similar results can be found in the aspect of the synchronization performance of the control system. Note that the magnitudes of the faults in two HA channels are not the same and this may lead to a more serious force fighting problem. Moreover, the existence of large disturbances will make the problem worse. Therefore, the algorithm which incorporates faults and disturbances compensation will improve the synchronization performance of the system. As shown in Figure 4 and Table 3, during the fault-transient time, the maximum fighting force for DAFTSC is 4.1716e+003N, the smallest of the four algorithms.

After experiencing a fault transient time, the faulty system enters into the steady state. During this time period, the position tracking accuracy of the closed-loop system is mainly affected by the faults. Therefore, the algorithms with fault

TABLE 3. Indexes for measurement of system synchronization performance for four algorithms.

Algorithms	Steady state before fault occurrence $t \in [5s, 10s)$			Fault Transient $t \in [10s, 11s)$	Steady state after fault occurrence $t \in [25s, 30s)$		
	M_f (N)	μ_f (N)	σ_f (N)	M_f (N)	M_f (N)	μ_f (N)	σ_f (N)
RSC	2.6338e+003	1.2479e+003	799.2289	2.0298e+004	2.0613e+004	1.3411e+004	6.2426e+003
DSC	272.8188	36.8442	25.6461	8.1328e+003	8.2034e+003	3.4791e+003	1.8888e+003
AFTSC	530.3088	339.7230	176.8424	2.2126e+004	4.1941e+003	582.0500	784.9022
DAFTSC	273.4514	36.8973	25.9278	4.1716e+003	4.6103e+003	217.5879	500.1590

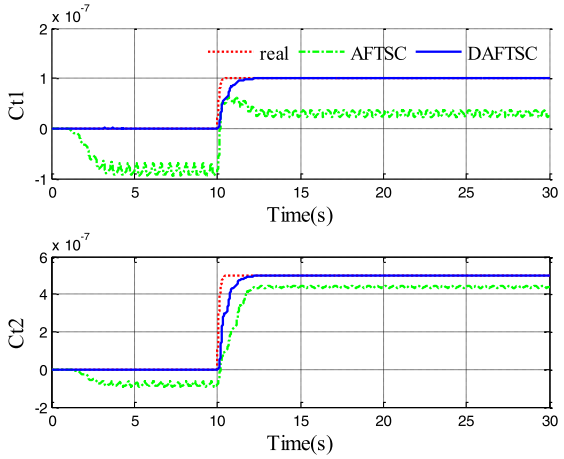

FIGURE 5. Estimations of internal leakage faults in two HA channels.

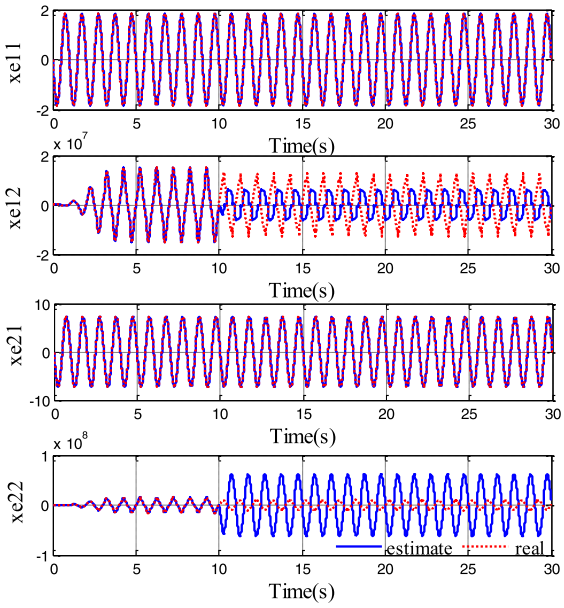

FIGURE 6. Estimations of the matched and unmatched disturbances in two HA channels by using the DSC algorithm.

estimation and compensation ability exhibit better position tracking performance. According to Table 2, the average position tracking errors of the algorithms DAFTSC and AFTSC are 5.2185e − 005 rad and 4.7411e −004 rad respectively, less than the other two algorithms. Moreover, the DAFTSC

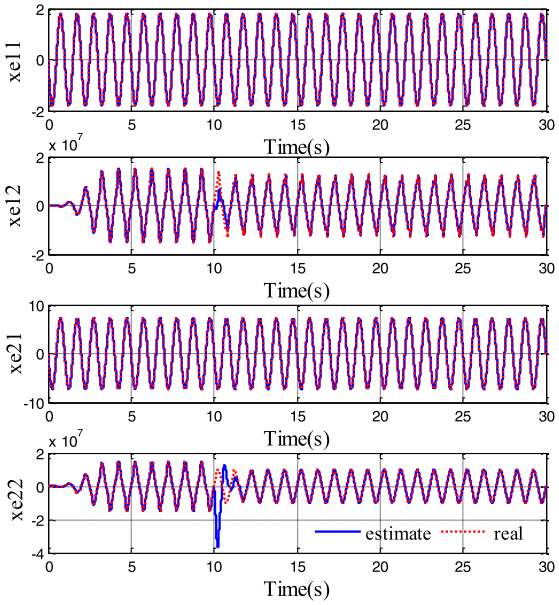

FIGURE 7. Estimations of the matched and unmatched disturbances in two HA channels by using the proposed DAFTSC algorithm.

algorithm outperforms the AFTSC algorithm for all positon tracking performance indexes due to its disturbance rejection ability. As shown in Table 3, similar results can be found in the aspect of the synchronization performance of the faulty system.

Remark 8: In normal condition, the unequal disturbances d_1 and d_2 make differences in displacement dynamics between two HAs and the differences are the most obvious as the piston velocity of each hydraulic cylinder changes its direction. For DSC and DAFTSC, the positon tracking errors (or the fighting force) caused by the displacement differences are greatly reduced by employing the disturbance estimation and compensation strategy. However, as shown in Figure 3 and Figure 4, the curves of the position tracking error (or the fighting force) for DSC and DAFTSC still exhibit some "glitches" when the piston velocity of the hydraulic cylinder experiences a direction change. Similar results can be found after the occurrence of the faults, and during this period, the differences of the displacement dynamics are mainly caused by the unequal faults in two HAs.

Figure 5 compares the faulty parameter estimation results for the algorithms DAFTSC and AFTSC. For the proposed

DAFTSC algorithm, estimations of the internal leakage faults in two HA channels converge to their real values at about $t = 12s$. In contrast, the AFTSC algorithm has constant estimation error during the whole estimation process under the influence of large disturbances.

The estimation results of the matched and unmatched disturbances in two HA channels for the algorithms DSC and DAFTSC are presented in Figure 6 and Figure 7, respectively. According to (21), the faults appear in the same equation as the matched disturbances and thus mainly affect the estimation accuracy of the matched disturbances. As shown in the second and fourth subgraphs of Figure 6, the matched disturbance estimations of the DSC algorithm deviate from their true values immediately after the occurrence of the faults, for the disturbance observers (32) employed in this algorithm do not have parameters updating online. In comparison, the disturbance estimations of the DAFTSC algorithm gradually converge to their real values with the convergence of the faulty parameter estimations.

V. CONCLUSION

In this paper, a fault-tolerant synchronization control algorithm based on adaptive backstepping technology and disturbances estimation is proposed to handle the control problem of a DRHAS on A/A mode in the face of internal leakage faults, large disturbances and force fighting problem. To achieve positon tracking and force outputs synchronization simultaneously, two reference trajectories are introduced and a novel nonlinear model of the DRHAS is developed. Based on the backstepping method, a nonlinear controller incorporating the adaptive control and the observer-based disturbance rejection control is proposed. In which, the internal leakage faults are accommodated by a simple reconfiguration strategy based on faulty parameter online adaptation, and the matched and unmatched disturbances are estimated by four ESOs and are compensated in a feedforward way. Comparative simulation results finally demonstrate the effectiveness of the proposed control algorithm.

Since the proposed control algorithm is designed based on full-state feedback, future study will focus on the development of an output-feedback FTSC algorithm for the DRHAS under the condition that only the displacement signals in both HAs are measurable. Moreover, how to design a control scheme to handle the fault-tolerant synchronization problem for the DRHAS in the present of time-varying disturbances to achieve asymptotic stability needs to be investigated.

REFERENCES

[1] D. Briere and P. Traverse, "AIRBUS A320/A330/A340 electrical flight controls—A family of fault-tolerant systems," in *Proc. 23rd Int. Symp. Fault-Tolerant Comput. (FTCS)*, Toulouse, France, Jun. 1993, pp. 616–623.

[2] D. R. Ryder, "Redundant actuator development study," Boeing Commercial Airplane Corp., Seattle, WA, USA, Tech. Rep. CR-114730, 1973.

[3] Y. Fu, Y. Pang, H. Liu, and Y. Zhang, "Force fighting research of dual redundant hydraulic actuation system," in *Proc. ISDEA*, Changsha, China, Oct. 2011, pp. 762–766.

[4] G. Jacazio and L. Gastaldi, "Equalization techniques for dual redundant electro hydraulic servo actuator for flight control systems," in *Proc. FPMC*, Bath, U.K., Sep. 2008, pp. 543–557.

[5] C. Shi, X. Wang, S. Wang, J. Wang, and M. M. Tomovic, "Adaptive decoupling synchronous control of dissimilar redundant actuation system for large civil aircraft," *Aerosp. Sci. Technol.*, vol. 47, pp. 114–124, Dec. 2015.

[6] O. Cochoy, S. Hanke, and U. B. Carl, "Concepts for position and load control for hybrid actuation in primary flight controls," *Aerosp. Sci. Technol.*, vol. 11, nos. 2–3, pp. 194–201, Mar./Apr. 2007.

[7] X. Wang, C. Shi, and S. Wang, "Extended state observer-based motion synchronisation control for hybrid actuation system of large civil aircraft," *Int. J. Syst. Sci.*, vol. 48, no. 10, pp. 2212–2222, Mar. 2017.

[8] L. Chen, "Model-based fault diagnosis and fault-tolerant control for a nonlinear electro-hydraulic system," Ph.D. dissertation, Dept. Elect. Inf. Eng., TU Kaiserslautern, Kaiserslautern, Germany, 2010.

[9] L. An and N. Sepehri, "Leakage fault detection in hydraulic actuators subject to unknown external loading," *Int. J. Fluid Power*, vol. 9, no. 2, pp. 15–25, Jun. 2008.

[10] M. Sepasi and F. Sassani, "On-line fault diagnosis of hydraulic systems using unscented Kalman filter," *Int. J. Control, Autom. Syst.*, vol. 8, no. 1, pp. 149–156, 2010.

[11] A. Y. Goharrizi and N. Sepehri, "A wavelet-based approach for external leakage detection and isolation from internal leakage in valve-controlled hydraulic actuators," *IEEE Trans. Ind. Electron.*, vol. 58, no. 9, pp. 4374–4384, Sep. 2011.

[12] Z. Yao, Y. Yu, and J. Yao, "Artificial neural network–based internal leakage fault detection for hydraulic actuators: An experimental investigation," *Proc. Inst. Mech. Eng. I, J. Syst. Control Eng.*, vol. 232, no. 4, pp. 369–382, Apr. 2018.

[13] Q. N. Xu, K. M. Lee, H. Zhou, and H. Y. Yang, "Model-based fault detection and isolation scheme for a rudder servo system," *IEEE Trans. Ind. Electron.*, vol. 62, no. 4, pp. 2384–2396, Apr. 2015.

[14] V. Mahulkar, D. E. Adams, and M. Derriso, "Adaptive fault tolerant control for hydraulic actuators," in *Proc. ACC*, Chicago, IL, USA, Jul. 2015, pp. 2242–2247.

[15] J. Yao, G. Yang, and D. Ma, "Internal leakage fault detection and tolerant control of single-rod hydraulic actuators," *Math. Problems Eng.*, vol. 2014, Mar. 2014, Art. no. 345345.

[16] M. Karpenko and N. Sepehri, "Robust position control of an electrohydraulic actuator with a faulty actuator piston seal," *ASME J. Dyn. Syst., Meas., Control*, vol. 125, pp. 413–423, Sep. 2003.

[17] Z. Zhao, "Active fault tolerant control of an electro-hydraulic driven elevator based on robust adaptive observers," Ph.D. dissertation, Dept. Mech. Ind. Eng., Concordia Univ., Montreal, QC, Canada, 2010.

[18] C. Shi, S. Wang, X. Wang, J. Wang, and M. M. Tomovic, "Active fault-tolerant control of dissimilar redundant actuation system based on performance degradation reference models," *J. Franklin Inst.*, vol. 354, no. 2, pp. 1087–1108, Jan. 2017.

[19] A. S. Kaya and M. Z. Bilgin, "Output feedback control surface positioning with a high-order sliding mode controller/estimator: An experimental study on a hydraulic flight actuation system," *J. Dyn. Syst. Meas. Control*, vol. 141, no. 1, Jan. 2019, Art. no. 011009.

[20] Z. Has, M. F. Rahmat, A. R. Husain, and M. N. Ahmad, "Robust precision control for a class of electro-hydraulic actuator system based on disturbance observer," *Int. J. Precis. Eng. Manuf.*, vol. 16, no. 8, pp. 1753–1760, Jul. 2015.

[21] J. Yao, Z. Jiao, and D. Ma, "A practical nonlinear adaptive control of hydraulic servomechanisms with periodic-like disturbances," *IEEE/ASME Trans. Mechatronics*, vol. 20, no. 6, pp. 2752–2760, Dec. 2015.

[22] K. Guo, J. Wei, J. Fang, R. Feng, and X. Wang, "Position tracking control of electro-hydraulic single-rod actuator based on an extended disturbance observer," *Mechatronics*, vol. 27, pp. 47–56, Apr. 2015.

[23] W. Kim, D. Shin, D. Won, and C. C. Chung, "Disturbance-observer-based position tracking controller in the presence of biased sinusoidal disturbance for electrohydraulic actuators," *IEEE Trans. Control Syst. Technol.*, vol. 21, no. 6, pp. 2290–2298, Nov. 2013.

[24] D. Won, W. Kim, D. Shin, and C. C. Chung, "High-gain disturbance observer-based backstepping control with output tracking error constraint for electro-hydraulic systems," *IEEE Trans. Control Syst. Technol.*, vol. 23, no. 2, pp. 787–795, Mar. 2015.

[25] Z. Yao, J. Yao, and W. Sun, "Adaptive RISE control of hydraulic systems with multilayer neural-networks," *IEEE Trans. Ind. Electron.*, to be published. doi: 10.1109/TIE.2018.2886773.

[26] J. Yao and W. Deng, "Active disturbance rejection adaptive control of hydraulic servo systems," *IEEE Trans. Ind. Electron.*, vol. 64, no. 10, pp. 8023–8032, Oct. 2017.
[27] B. Ayalew and B. T. Kulakowski, "Cascade tuning for nonlinear position control of an electrohydraulic actuator," in *Proc. ACC*, Minneapolis, MN, USA, Jun. 2006, p. 6.
[28] J. Yao, Z. Jiao, D. Ma, and L. Yan, "High-accuracy tracking control of hydraulic rotary actuators with modeling uncertainties," *IEEE/ASME Trans. Mechatronics*, vol. 19, no. 2, pp. 633–641, Apr. 2014.
[29] T. Li, X. Wang, T. Yang, Y. Cao, and R. Xie, "Adaptive robust fault-tolerant synchronization control for a dual redundant hydraulic actuation system with common-mode fault," *Math. Problems Eng.*, vol. 2018, Oct. 2018, Art. no. 6570104.
[30] B. Yao and M. Tomizuka, "Adaptive robust control of SISO nonlinear systems in a semi-strict feedback form," *Automatica*, vol. 33, no. 5, pp. 893–900, May 1997.
[31] S. E. Talole, J. P. Kolhe, and S. B. Phadke, "Extended-state-observer-based control of flexible-joint system with experimental validation," *IEEE Trans. Ind. Electron.*, vol. 57, no. 4, pp. 1411–1419, Apr. 2010.
[32] B.-Z. Guo and Z.-L. Zhao, "On the convergence of an extended state observer for nonlinear systems with uncertainty," *Syst. Control Lett*, vol. 60, pp. 420–430, Jun. 2011.
[33] B. Yao, F. Bu, J. Reedy, and G. T. C. Chiu, "Adaptive robust motion control of single-rod hydraulic actuators: Theory and experiments," *IEEE/ASME Trans. Mechatronics*, vol. 5, no. 1, pp. 79–91, Mar. 2000.
[34] M. Hou, G. Duan, and M. Guo, "New versions of Barbalat's lemma with applications," *J. Control Theory Appl.*, vol. 8, no. 4, pp. 545–547, Nov. 2010.
[35] Y.-X. Li and G.-H. Yang, "Fuzzy adaptive output feedback fault-tolerant tracking control of a class of uncertain nonlinear systems with nonaffine nonlinear faults," *IEEE Trans. Fuzzy Syst.*, vol. 24, no. 1, pp. 223–234, Feb. 2016.
[36] J. Yao, Z. Jiao, and D. Ma, "Extended-state-observer-based output feedback nonlinear robust control of hydraulic systems with backstepping," *IEEE Trans. Ind. Electron.*, vol. 61, no. 11, pp. 6285–6293, Nov. 2014.

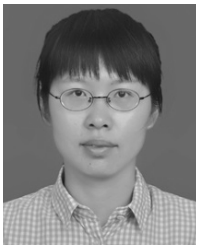

TING LI received the master's degree in control theory and control engineering, in 2008. She is currently pursuing the Ph.D. degree with the School of Automation, Northwestern Polytechnical University, Xi'an, China. Her research interests include fault diagnosis and fault-tolerant control for dual redundant hydraulic actuation systems.

TING YANG received the M.S. and Ph.D. degrees in control science and engineering from the Harbin Institute of Technology, Harbin, China, in 2011 and 2016, respectively. From 2013 to 2015, she was a Visiting Scholar with the Department of Mechanical and Aerospace Engineering, North Carolina State University, Raleigh, NC, USA. She is currently an Assistant Professor with the School of Automation, Northwestern Polytechnical University, Xi'an, China. Her research interests include nondeterministic and stochastic switching systems, fuzzy control systems, model predictive control, and their applications.

YUYAN CAO received the B.S. degree in automation from Northwestern Polytechnical University, Xi'an, China, in 2013, where she is currently pursuing the Ph.D. degree in control theory and control engineering. Her current research interests include fault diagnosis and fault prediction for aircraft actuation systems.

RONG XIE received the M.S. and Ph.D. degrees in control science and engineering from Northwestern Polytechnical University, Xi'an, China, in 2006 and 2009, respectively, where she is currently an Associate Professor with the School of Automation. Her research interests include probabilistic robust control and fault-tolerant control for the aircraft actuation systems.

XINMIN WANG received the B.S. degree from Norhwestern Polytechnical University, Xi'an, China, and the M.S. degree from the Nanjing University of Science and Technology. He is currently a Professor with the School of Automation, Northwestern Polytechnical University. His research interests include flight control system design, fault diagnosis, and fault tolerant-control for aircraft actuation systems.